

Residual Multi-Fidelity Neural Network Computing

Owen Davis^{*1}, Mohammad Motamed^{†1}, and Raúl Tempone^{‡2,3}

¹*Department of Mathematics and Statistics, The University of New Mexico, Albuquerque, USA*

²*Computer, Electrical and Mathematical Sciences and Engineering Division (CEMSE), King Abdullah University of Science and Technology (KAUST), Thuwal, Saudi Arabia*

³*Alexander von Humboldt Professor in Mathematics for Uncertainty Quantification, RWTH Aachen University, Aachen, Germany*

Dedicated to the memory of Ivo Bubuska

Abstract

In this work, we consider the general problem of constructing a neural network surrogate model using multi-fidelity information. Motivated by error-complexity estimates for ReLU neural networks, we formulate the correlation between an inexpensive low-fidelity model and an expensive high-fidelity model as a possibly non-linear residual function. This function defines a mapping between 1) the shared input space of the models along with the low-fidelity model output, and 2) the discrepancy between the outputs of the two models. The computational framework proceeds by training two neural networks to work in concert. The first network learns the residual function on a small set of high- and low-fidelity data. Once trained, this network is used to generate additional synthetic high-fidelity data, which is used in the training of the second network. The trained second network then acts as our surrogate for the high-fidelity quantity of interest. We present four numerical examples to demonstrate the power of the proposed framework, showing that significant savings in computational cost may be achieved when the output predictions are desired to be accurate within small tolerances.

keywords: multi-fidelity computing, residual modeling, deep neural networks, uncertainty quantification

MSC 2020: 65C30, 65C40, 68T07

1 Introduction

Deep artificial neural networks are widely regarded as central tools to solve a variety of artificial intelligence problems; see e.g. [1] and the references therein. The application of neural networks is, however, not limited to artificial intelligence. In recent years, deep networks have been successfully used to construct fast-to-evaluate surrogates for physical/biological quantities of interest (QoIs) described by complex systems of ordinary/partial differential equations (ODEs/PDEs); see e.g. [2, 3, 4]. This has resulted in a growing body of research on the integration of physics-based modeling

*corresponding author: address: University of New Mexico Department of Mathematics and Statistics 311 Terrace Street NE, Room 389 Albuquerque, NM, USA 87106, email: davis@unm.edu

†motamed@unm.edu

‡raul.tempone@kaust.edu.sa

with neural networks [5]. As surrogate models, deep networks have several important properties: 1) their expressive power enables them to accurately approximate a wide class of functions; see e.g. [6, 7, 8, 9, 10, 11, 12, 13]; 2) they can handle high-dimensional parametric problems involving many input parameters; see e.g. [14, 15, 16, 17, 18]; and 3) they are fast-to-evaluate surrogates, as their evaluations mainly require simple matrix-vector operations. Despite possessing such desirable properties, deep network surrogates are often very expensive to construct, especially when high levels of accuracy are desired [19] and the underlying ODE/PDE systems are expensive to compute accurately. The construction of deep networks often requires abundant high-fidelity training data that in turn necessitates many expensive high-fidelity ODE/PDE computations.

To address this issue, we put forth a residual multi-fidelity computational framework. Given a low-fidelity and a high-fidelity computational model, we formulate the relation between the two models in terms of a residual function. This function is defined as a possibly non-linear mapping between 1) the shared input space of the models together with the low-fidelity model output and 2) the discrepancy between the two model outputs. This formulation is motivated by a recent theoretical result [13], which shows that for a large class of bounded target functions with minimal regularity assumptions there exists a ReLU network whose approximation error is bounded above by a quantity proportional to the uniform norm of the target function and inversely proportional to the network complexity. As such, given a specified network error tolerance, and assuming the discrepancy between model outputs has a small uniform norm relative to the high-fidelity quantity, the residual framework allows the relationship between models of different fidelity to be learned within the desired accuracy using a network of lower complexity. This approach, in contrast to directly learning the mapping between models, reduces the amount of training data required, thus making it less costly to acquire. The trained network is then used as a surrogate to efficiently generate additional high-fidelity data. Finally, the enlarged set of originally available and newly generated high-fidelity data is used to train a deep network that learns, and acts as a fast-to-evaluate surrogate, for the high-fidelity QoI. We present four numerical examples to demonstrate the power of the proposed framework. In particular, we show that significant savings in computational cost may be achieved when the discrepancy between models is small in uniform norm and the output predictions are desired to be accurate within small tolerances.

We remark as well that the developed framework is not limited to bi-fidelity modeling; it extends naturally to multi-fidelity modeling problems where the ensemble of lower-fidelity models are strictly hierarchical in terms of their predictive utility per cost. To accomplish this extension a sequence of networks learns a sequence of residuals that move up the model hierarchy.

Related work. This work introduces a neural network-driven computational framework that leverages multi-fidelity information and residual modeling, bolstered by recent bounds on network approximation error and complexity [13]. Multi-fidelity modeling with neural networks is a quickly growing research area with numerous recent works; see e.g., [20, 21, 22, 23, 24, 25, 26, 27, 28, 29]. In [20, 21, 23], standard feedforward networks are used to directly learn the correlation between the low- and high-fidelity model, but make different a-priori assumptions concerning the form of this correlation. The authors in [22, 27] leverage physics-informed networks for this multi-fidelity learning task, and the latter further utilizes operator learning frameworks. In [25], several neural network modeling frameworks are proposed that leverage connections between neural network approximation and Gaussian process regression. The authors in [29] tackle this multi-fidelity learning problem using convolutional encoder/decoder networks, and in [28] multi-fidelity information is utilized together with long short-term memory networks. In [24] a multi-fidelity Bayesian neural network framework is developed, and finally, in [26] multi-fidelity information is harnessed via a

transfer learning approach. Many of these modeling paradigms have been empirically successful, but theoretical analysis that clarifies under what modeling conditions they are performative is generally intractable. In this way, the present work is different. Our modeling paradigm is inspired by the ReLU network approximation error-complexity estimate proved in [13], which provides high-level guidelines concerning the modeling conditions required for the developed computational framework to be performative. Importantly, the purpose of this work is not to develop a neural network modeling paradigm and provide exhaustive numerical comparison with the existing methods in the literature. Rather, our main objective is to develop a theoretically supported modeling paradigm and verify numerically that it performs well under the predicted conditions.

Our work also leverages a type of residual modeling, but unlike most residual modeling approaches, where the residual is often defined as the difference of observed and simulated data (see e.g. [30]), we define the residual as the discrepancy between high- and low-fidelity data. Our framework is also different from recent reduced-order modeling approaches (see e.g. [31]) that utilize residuals to measure the discrepancy between full-order and reduced-order models. While in these approaches residuals account for model reduction due to modal decomposition and truncation, i.e. residuals gauge the discarded modes in the original full-order model, we define residuals as the difference between the target output QoIs at different levels of fidelity. A similar residual modeling strategy to our framework can be found in residual networks (ResNets) [32], where a residual function is defined as the difference between the output and input of a block of neural layers. Our framework adds a systematic inclusion of multi-fidelity modeling to ResNets; see a more detailed discussion on ResNets in Section 3.2.

The rest of the paper is organized as follows. In Section 2, we state the mathematical formulation of the problem. In Section 3, we present the residual multi-fidelity neural network algorithm and show how it is rigorously motivated by recently proved theoretical results in [13]. In Section 4, we discuss sources of error and computational complexity in the developed algorithm. In Section 5, we present four numerical examples that demonstrate the power of the proposed framework. Finally, in Section 6, we conclude and outline future works.

2 Problem formulation and background

In this section, we formulate the problem and provide a brief overview of multi-fidelity modeling and ReLU neural networks, laying the necessary groundwork for the subsequent material.

2.1 Problem statement

Let $\mathbf{u} : (\mathbf{x}, \boldsymbol{\theta}) \in X \times \Theta \subset \mathbb{R}^n \times \mathbb{R}^d \mapsto \mathbf{u}(\mathbf{x}; \boldsymbol{\theta}) \in \mathbb{R}^m$ be the solution to a (computationally involved) system of parametric ODEs/PDEs, parameterized by $\boldsymbol{\theta} \in \Theta \subset \mathbb{R}^d$. Further, let $Q : \Theta \rightarrow \mathbb{R}$ be a target function defined as a functional or operator, M_Q , acting on \mathbf{u} ,

$$Q : \boldsymbol{\theta} \in \Theta \subset \mathbb{R}^d \mapsto Q(\boldsymbol{\theta}) \in \mathbb{R}, \quad Q(\boldsymbol{\theta}) = M_Q(\mathbf{u}(\mathbf{x}; \boldsymbol{\theta})).$$

For example, the target function Q may be given by the ODE/PDE solution energy, where $M_Q(\mathbf{u}(\mathbf{x}; \boldsymbol{\theta})) = \int_X |\mathbf{u}(\mathbf{x}; \boldsymbol{\theta})|^2 d\mathbf{x}$. In general, since the target quantity Q is available to us through a set of ODEs/PDEs, we may assume that it belongs to some Sobolev space.

Suppose that we need many accurate evaluations of $Q(\boldsymbol{\theta})$ at many distinct points $\boldsymbol{\theta} \in \Theta$. Such a situation arises, for example, in forward and inverse uncertainty quantification (UQ). In principle, direct evaluations/realizations of Q will require a very large number of expensive high-fidelity ODE/PDE computations that may be computationally prohibitive. Therefore, our goal is

to construct a fast-to-evaluate surrogate of the target function Q , say \tilde{Q} , using only a small number of expensive simulations of high-fidelity ODE/PDE models, and satisfying the accuracy constraint

$$\varepsilon := \|Q - \tilde{Q}\|_{L^p_\pi(\Theta)} = \left(\int_{\Theta} |Q(\boldsymbol{\theta}) - \tilde{Q}(\boldsymbol{\theta})|^p d\pi(\boldsymbol{\theta}) \right)^{1/p} \leq \varepsilon_{TOL}. \quad (1)$$

Here, we measure the approximation error in the L^p -norm, with $p \in [1, \infty)$ and weighted with a probability measure $d\pi$ on Θ , and $\varepsilon_{TOL} \in (0, 1/2)$ is a desired small tolerance. As we will show in Section 3, we will achieve this goal by introducing a residual multi-fidelity framework that exploits the approximation power of deep networks and the efficiency of approximating quantities of small uniform norm. Once constructed, the surrogate can be combined with Monte Carlo (MC) and collocation methods (see e.g. [33, 34, 35, 36]) to compute the statistics of the QoI; see the numerical examples in Section 5.

The new framework has two major components: i) multi-fidelity modeling; and ii) neural network approximation. We will briefly review these components in the remainder of this section.

2.2 Multi-fidelity modeling

The basic idea of multi-fidelity modeling is to leverage models at different levels of fidelity in order to achieve a desired accuracy with minimal computational cost. Let $Q_{LF}(\boldsymbol{\theta})$ and $Q_{HF}(\boldsymbol{\theta})$ be two approximations of the target quantity $Q(\boldsymbol{\theta})$, obtained by a low-fidelity and a high-fidelity computational model, satisfying the following two assumptions:

- A1.** Q_{HF} is a computationally expensive approximation of Q , satisfying (1) with $\tilde{Q} = Q_{HF}$;
- A2.** Q_{LF} is a computationally cheaper but less accurate approximation of Q , which is correlated with Q_{HF} .

One common modeling scenario that can satisfy assumptions **A1-A2** occurs when the high- and low-fidelity models are built, respectively, from fine and coarse discretizations of the underlying ODE/PDE model. Specifically, suppose that

$$Q_{LF}(\boldsymbol{\theta}) := M_Q(\mathbf{u}_{h_{LF}}(\mathbf{x}; \boldsymbol{\theta})), \quad Q_{HF}(\boldsymbol{\theta}) = M_Q(\mathbf{u}_{h_{HF}}(\mathbf{x}; \boldsymbol{\theta})), \quad h_{HF} < h_{LF}, \quad (2)$$

where h_{LF} and h_{HF} denote the mesh size and/or the time step of a stable discretization scheme used at the low fidelity and high-fidelity levels, respectively. Assume further that

$$|Q(\boldsymbol{\theta}) - Q_{LF}(\boldsymbol{\theta})| \leq c(\boldsymbol{\theta}) h_{LF}^q, \quad |Q(\boldsymbol{\theta}) - Q_{HF}(\boldsymbol{\theta})| \leq c(\boldsymbol{\theta}) h_{HF}^q, \quad \forall \boldsymbol{\theta} \in \Theta, \quad (3)$$

where $q > 0$ is related to the order of accuracy of the discretization scheme, and $c = c(\boldsymbol{\theta}) > 0$ is a bounded function. Then this upper error bound implies that assumptions **A1-A2** can be satisfied with proper choices of h_{LF} and h_{HF} , e.g. with $h_{HF} \propto \varepsilon_{TOL}^{1/q}$ and h_{LF} small enough for Q_{LF} to be correlated with Q_{HF} .

This example is intuitive and admits a very clear and mathematically rigorous notion of high- and low-fidelity, but importantly, it is not the only option. Lower-fidelity models can also be generated by solving an auxiliary problem obtained by simplifying the original problem. For instance, we may consider a model with simpler physics, an effective model derived through homogenization, or a reduced model obtained by smoothing out the rough parameters of M_Q , linearization, or modal decomposition and truncation. In this work, we primarily consider lower-fidelity models

obtained by solving the underlying system of differential equations on a coarser discretization, but we additionally, in Section 5.2, deploy the developed modeling framework on a test problem where the low-fidelity model is obtained by asymptotic approximation.

It is to be noted that in general the selection of low-fidelity and high-fidelity models is problem dependent. We consider a set of multi-fidelity models admissible as long as assumptions **A1-A2** are satisfied, but we note that satisfying **A1-A2** is not sufficient to guarantee that the chosen multi-fidelity models are optimal in terms of computational efficiency for a desired accuracy.

The pivotal step in multi-fidelity computation is to design a procedure that captures and utilizes the relationship between models at different levels of fidelity. One of the most established approaches uses a Bayesian auto-regressive Gaussian process (GP) [37, 38]. This method works well for sparse high-fidelity data, but is often computationally prohibitive for high dimensional problems. It is in this high dimensional regime that neural network based multi-fidelity surrogate modeling promises to make an impact. A widely used neural network based approach, known as *comprehensive correction*, assumes a linear correlation between models, writing $Q_{HF}(\boldsymbol{\theta}) = \rho(\boldsymbol{\theta})Q_{LF}(\boldsymbol{\theta}) + \delta(\boldsymbol{\theta})$, where ρ and δ are the unknown multiplicative and additive corrections, respectively; see e.g. [39]. The main limitation of this strategy is its inability to capture a possibly nonlinear correlations between the two models. In certain regions of the domain Θ , where the two models lack a strong linear correlation—such as in time-dependent problems where the low-fidelity data deteriorates and diverges from the high-fidelity data over time—a linear formulation may disregard the low-fidelity model (which could still provide valuable information) and assign all the weight to the high-fidelity data; see also Figure 1. In order to address this limitation, more general approaches have been proposed. In [40], the authors replace the linear multiplicative relation by a nonlinear one and consider $Q_{HF}(\boldsymbol{\theta}) = F(Q_{LF}(\boldsymbol{\theta})) + \delta(\boldsymbol{\theta})$, where F is a (possibly nonlinear) unknown function. Other related works that also employ neural networks to construct multi-fidelity regression models include [22, 23]. In [22], a combination of linear and nonlinear relations between models, $Q_{HF}(\boldsymbol{\theta}) = F_L(\boldsymbol{\theta}, Q_{LF}(\boldsymbol{\theta})) + F_{NL}(\boldsymbol{\theta}, Q_{LF}(\boldsymbol{\theta}))$ is used, and [23] utilizes a general correlation between the two models, $Q_{HF}(\boldsymbol{\theta}) = F(\boldsymbol{\theta}, Q_{LF}(\boldsymbol{\theta}))$, with F being a general nonlinear unknown function. These formulations however are not capable of exploiting the full potential of multi-fidelity modeling to gain computational efficiency.

Motivated by residual modeling, instead of searching for a direct correlation between models, we reformulate the correlation in terms of a (possibly nonlinear) residual function that measures the discrepancy between the models; see Section 3.1. We will show how and why such a formulation can achieve higher levels of efficiency.

2.3 Neural network approximation

Deep neural network surrogates can be very expensive to construct [19], especially when high levels of accuracy are desired and the underlying ODE/PDE systems, that generate high-fidelity training data, are expensive to compute accurately. Although ResNets [32] alleviate this issue to some extent by addressing the *degradation* problem (as depth increases, accuracy degrades), this work takes a step further by leveraging a combination of deep networks and cheap low-fidelity computations to efficiently build deep high-fidelity networks. We will specifically focus on ReLU feedforward networks, possibly augmented with a ResNet style architecture, as defined below.

ReLU networks. Following the setup used in [41, 12], we define a feedforward network with $N_0 = d$ inputs and L layers, each with N_ℓ neurons, $\ell = 1, \dots, L$, by a sequence of matrix-vector (or

weight-bias) tuples

$$\Phi := \{(W_1, b_1), \dots, (W_L, b_L)\}, \quad W_\ell \in \mathbb{R}^{N_\ell \times N_{\ell-1}}, \quad b_\ell \in \mathbb{R}^{N_\ell}, \quad \ell = 1, \dots, L.$$

We denote by f_Φ the function that the network Φ realizes and write,

$$f_\Phi(\boldsymbol{\theta}) = \mathbf{z}_L, \quad f_\Phi : \mathbb{R}^d \rightarrow \mathbb{R}^{N_L},$$

where \mathbf{z}_L results from the following scheme:

$$\mathbf{z}_0 = \boldsymbol{\theta}, \quad \mathbf{z}_\ell = \sigma(W_\ell \mathbf{z}_{\ell-1} + b_\ell), \quad \ell = 1, \dots, L-1, \quad \mathbf{z}_L = W_L \mathbf{z}_{L-1} + b_L.$$

Here, $\sigma : \mathbb{R} \rightarrow \mathbb{R}$ is the ReLU activation function $\sigma(z) = \max(0, z)$ that acts component-wise on all hidden layers, $\ell = 1, \dots, L-1$. To make this ReLU network a ReLU ResNet we simply add shortcut connections to this structure which pass along the identity map.

3 Residual multi-fidelity neural network algorithm

In this section, we present a residual multi-fidelity neural network (RMFNN) algorithm consisting of two major parts: 1) formulation of a new residual multifidelity framework, and 2) construction of a pair of neural networks that work in concert within the new framework. We will discuss each part in turn.

3.1 Nonlinear residual multi-fidelity modeling

Combining residual analysis and multi-fidelity modeling, we reformulate the mapping between two models of different fidelity as a non-linear residual function F and write

$$Q_{HF}(\boldsymbol{\theta}) - Q_{LF}(\boldsymbol{\theta}) = F(\boldsymbol{\theta}, Q_{LF}(\boldsymbol{\theta})), \quad \boldsymbol{\theta} \in \Theta. \quad (4)$$

As we will discuss below, this formulation enables the efficient construction of a fast-to-evaluate high-fidelity surrogate by a pair of neural networks that work in concert. The first network, which learns the residual function F is leveraged to train a second network that learns the high-fidelity target quantity Q_{HF} . The new formulation (4) is motivated by the following two observations.

I. Nonlinearity. In certain ODE/PDE problems, low-fidelity solutions lose their linear correlation with the high-fidelity solution on parts of the parameter domain. For example, in wave propagation problems, the low-fidelity solution may deteriorate as time increases due to dissipative and dispersive errors [42]. The low-fidelity solution may also deteriorate at low frequencies if it is obtained by the truncation of an asymptotic expansion that is valid at high frequencies [43]. As an illustrative example, consider a simple forced oscillator with damping given by the ODE system,

$$\dot{\mathbf{u}}(t) = A \mathbf{u}(t) + \cos(\theta t) \mathbf{b}, \quad \mathbf{u} = \begin{bmatrix} u_1 \\ u_2 \end{bmatrix}, \quad A = \begin{bmatrix} 0 & 1 \\ -3 & -3 \end{bmatrix}, \quad \mathbf{b} = \begin{bmatrix} 0 \\ 0.6 \end{bmatrix}.$$

Here, $\theta \in \Theta = [10, 50]$ is a frequency parameter. Let $Q(\theta) = u_2(T; \theta)^2$ be the desired quantity of interest, given by the square of the second component of ODE's solution at a terminal time $T = 1$. We use Forward Euler with a very small time step ($\Delta t = 10^{-6}$) to obtain a high-fidelity solution

$Q_{HF}(\theta)$. For the low-fidelity model, we employ an asymptotic method (see [43]), and noting that $\cos(\theta t) = (e^{i\theta t} + e^{-i\theta t})/2$, we consider the ansatz

$$\mathbf{u}(t) = \mathbf{u}_0(t) + \sum_{r=1}^{\infty} \frac{1}{\theta^r} \mathbf{u}_r(t; \theta), \quad \mathbf{u}_r(t; \theta) = \mathbf{u}_{r,-1}(t) e^{-i\theta t} + \mathbf{u}_{r,1}(t) e^{i\theta t}.$$

Inserting this ansatz into the ODE system and matching the terms with the same θ^{-r} and $e^{\pm i\theta t}$ coefficients, we truncate the infinite sum and keep the first term with $r = 1$. This yields the low-fidelity solution

$$\mathbf{u}(t) = \mathbf{u}_{LF}(t) + \mathcal{O}(\theta^{-2}), \quad \mathbf{u}_{LF}(t) = e^{tA} \mathbf{u}(0) + \frac{1}{\theta} \sin(\theta t) \mathbf{b}.$$

The high-fidelity solution is accurate but costly. The low-fidelity solution, having an explicit closed form, is cheap-to-compute, but it deteriorates when the frequency is low. Figure 1 (left) displays the deviation of Q_{LF} from Q_{HF} as the frequency decreases. In Figure 1 (middle) we observe that although the two models exhibit a rather linear relation for larger frequencies, at lower frequencies ($\theta < 30$) their relation is nonlinear. Hence for this system a purely linear auto-regressive approach would ignore Q_{LF} (that is still informative) in a large portion of the parameter domain Θ , instead putting all the weight on Q_{HF} . This would in turn increase the amount of (expensive) high-fidelity computations needed to build the surrogate model. On the contrary, the nonlinear formulation (4) has the capability of capturing more complex mappings, fully exploiting Q_{LF} .

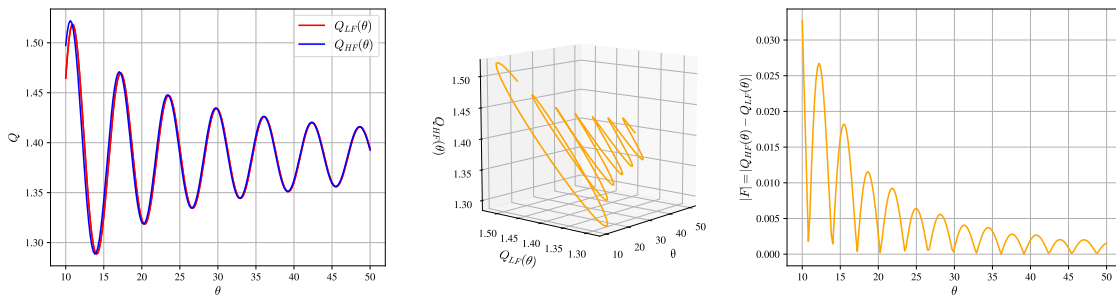


Figure 1: Motivation behind the new residual multi-fidelity formulation. Left: deviation of the low-fidelity solution Q_{LF} from the high-fidelity solution Q_{HF} , versus a frequency parameter $\theta \in \Theta = [10, 50]$. Middle: high-fidelity solution is not a linear function of the low-fidelity solution on the whole parameter space. Right: residual function F has a small magnitude.

II. Small residual magnitude. It is important to note that we do not formulate the non-linearity discussed above as a direct relation between the two models, that is, we do not write $Q_{HF}(\boldsymbol{\theta}) = F(\boldsymbol{\theta}, Q_{LF}(\boldsymbol{\theta}))$. Instead, we formulate the non-linearity in terms of the residual (4). This is motivated by a recently proved approximation error estimate in [13], which we include here as Theorem 1. In order to state the theorem rigorously, we define the space of target functions

$$S = \{Q : \mathbb{R}^d \rightarrow \mathbb{R} : \|Q\|_{L^1(\mathbb{R}^d)} < \infty, \|\hat{Q}\|_{L^1(\mathbb{R}^d)} < \infty, Q \not\equiv 0\}, \quad (5)$$

where \hat{Q} is the Fourier transform of Q . This space consists of all absolutely integrable functions on \mathbb{R}^d with absolutely integrable Fourier transform, excluding the identically zero function. Importantly, functions in S do not need to be continuous; they rather need to be continuous almost

everywhere. We remark here that when Q is discontinuous, we consider the relaxed notion of the Fourier transform [44], where it is only assumed that

$$Q(\boldsymbol{\theta}) = \int_{\mathbb{R}^d} \hat{Q}(\boldsymbol{\omega}) e^{i2\pi\boldsymbol{\omega}\cdot\boldsymbol{\theta}} d\boldsymbol{\omega} \quad \text{for almost every } \boldsymbol{\theta} \in \mathbb{R}^d.$$

Theorem 1. *Let $Q : \Theta \subseteq \mathbb{R}^d \rightarrow \mathbb{R}$ be a bounded function defined on the compact set Θ , and assume Q admits an extension $Q_e : \mathbb{R}^d \rightarrow \mathbb{R}$ such that $Q_e \in S$ and $\|Q_e\|_{L^\infty(\mathbb{R}^d)} \leq c\|Q\|_{L^\infty(\Theta)}$ for some $c \geq 0$. For any $\varepsilon \in (0, 1/2)$, there exists a ReLU network Q_Φ with depth $L \geq 2$, width $K > 2d + 2$, and satisfying:*

$$\|Q - Q_\Phi\|_{L^2(\Theta)} \leq \varepsilon, \tag{6}$$

such that

$$K L^{1/3} \leq C \|Q\|_{L^\infty(\Theta)}^2 \varepsilon^{-2} \log_2^{4/3}(\varepsilon^{-1}), \tag{7}$$

where C is a positive constant that may depend linearly on d and logarithmically on $\|Q\|_{L^\infty(\Theta)}$ and $\|\hat{Q}\|_{L^1(\mathbb{R}^d)}$.

Proof. For the proof we refer to [13]. □

Theorem 1 guarantees the existence of ReLU networks approximating a large class of bounded target functions with minimal regularity assumptions to arbitrary accuracy. Moreover, the required complexity of the approximating networks can be bounded above by a quantity proportional to the uniform norm of the target function and inversely proportional to a quantity that exhibits polynomial dependence on the desired tolerance. We note as well that the constant depends logarithmically on $\|\hat{Q}\|_{L^1(\mathbb{R}^d)}$, which can be understood as a weak dependence on target function regularity. Precisely, the Fourier transform of a function Q with integrable partial derivatives of order up to m decays like $|\hat{Q}| \sim \mathcal{O}(|\boldsymbol{\omega}|^{-m})$ [44], so the L^1 norm of the Fourier transform tends to increase with decreasing regularity. Importantly however, the constant C scales logarithmically with respect to $\|\hat{Q}\|_{L^1(\Theta)}$, so as the uniform norm of the target function becomes small, the dependence of the network complexity on target function size is dominated by $\|Q\|_{L^\infty}^2$.

This estimate highlights the potential of the residual modeling framework, particularly when the discrepancy between low- and high-fidelity models is small in uniform norm relative to the high-fidelity model. Under such conditions, the residual function can be approximated by a lower-complexity network, which we hypothesize will require less expensive high-fidelity training data. We support this hypothesis numerically in Section 5. Notably, we do not claim that the discrepancy is always smaller in uniform norm but suggest that the framework is especially effective when this condition holds.

An example where the uniform norm of the residual function is small is the wave propagation problem discussed earlier; see Figure 1. As an additional example, consider a pair of low- and high-fidelity models obtained by coarse and fine discretizations of an ODE/PDE problem, satisfying (3). Further, let $h_{LF} = s h_{HF}$ where $1 < s < \infty$. Then using triangle inequality we can write

$$\begin{aligned} |F| &= |Q_{HF} - Q_{LF}| \leq |Q - Q_{HF}| + |Q - Q_{LF}| \leq c(h_{HF}^q + h_{LF}^q) \\ &\leq c(1 + s^q)h_{HF}^q \leq (1 + s^q)\varepsilon_{TOL}. \end{aligned}$$

The last inequality follows from the choice $c h_{HF}^q \leq \varepsilon_{TOL}$, which implies that $\varepsilon := |Q - Q_{HF}| \leq \varepsilon_{TOL}$, as desired. Hence the size of the residual $|F|$ is proportional to the small quantity ε_{TOL} .

We remark here that Theorem 1 only guarantees the existence of neural networks satisfying the complexity estimate (7). It does not tell us how to find these networks. Hence an important assumption for the developed residual modeling framework is that we are able to successfully train neural networks that satisfy the approximation error estimate in Theorem 1.

In summary, the residual multi-fidelity formulation enables the construction of an efficient pair of networks where the first network, which learns the residual function F , is leveraged to train a second network that learns the target quantity Q_{HF} ; see Section 3.2 for details.

3.2 Composite network training

The second major component of the RMFNN algorithm involves constructing a pair of networks that work together. This construction proceeds in three steps.

Step 1. Data generation. We generate a set of $N = N_I + N_{II}$ points, $\boldsymbol{\theta} \in \Theta$, collected in two disjoint sets:

$$\Theta_I := \{\boldsymbol{\theta}^{(1)}, \dots, \boldsymbol{\theta}^{(N_I)}\} \subset \Theta, \quad \Theta_{II} := \{\boldsymbol{\theta}^{(N_I+1)}, \dots, \boldsymbol{\theta}^{(N)}\} \subset \Theta, \quad \Theta_I \cap \Theta_{II} = \emptyset.$$

The points in each set may be selected deterministically or randomly. For example, the two sets may consist of two uniform or non-uniform disjoint grids over Θ , or we may consider a random selection of points drawn from a probability distribution, such as a uniform distribution or other optimally chosen distribution. We then proceed with the following computations.

- For each $\boldsymbol{\theta}^{(i)} \in \Theta_I \cup \Theta_{II}$, with $i = 1, \dots, N$, we compute the low-fidelity realizations,

$$Q_{LF}^{(i)} := Q_{LF}(\boldsymbol{\theta}^{(i)}) = M_Q(\mathbf{u}_{h_{LF}}(\mathbf{x}; \boldsymbol{\theta}^{(i)})), \quad i = 1, \dots, N.$$

- For each $\boldsymbol{\theta}^{(i)} \in \Theta_I$, with $i = 1, \dots, N_I$, we compute the high-fidelity realizations,

$$Q_{HF}^{(i)} := Q_{HF}(\boldsymbol{\theta}^{(i)}) = M_Q(\mathbf{u}_{h_{HF}}(\mathbf{x}; \boldsymbol{\theta}^{(i)})), \quad i = 1, \dots, N_I. \quad (8)$$

Step 2. Composite network training. We train two separate networks as follows:

- Using N_I input data, $\{(\boldsymbol{\theta}^{(i)}, Q_{LF}^{(i)})\}_{i=1}^{N_I}$ and N_I output data, $\{Q_{HF}^{(i)} - Q_{LF}^{(i)}\}_{i=1}^{N_I}$, we train an initial network (*ResNN*) to learn the residual function F in (4). We call this surrogate F_{ResNN} ; see Figure 2 (top).
- We then use the surrogate F_{ResNN} and the rest of the N_{II} low-fidelity data points $\{(\boldsymbol{\theta}^{(i)}, Q_{LF}^{(i)})\}_{i=N_I+1}^N$ to generate N_{II} new approximate high-fidelity outputs, denoted by $\{\bar{Q}_{HF}^{(i)}\}_{i=N_I+1}^N$, where

$$\bar{Q}_{HF}^{(i)} := Q_{LF}^{(i)} + F_{ResNN}(\boldsymbol{\theta}^{(i)}, Q_{LF}^{(i)}), \quad i = N_I + 1, \dots, N. \quad (9)$$

- Using all N input-output high-fidelity data $\{(\boldsymbol{\theta}^{(i)}, Q_{HF}^{(i)})\}_{i=1}^{N_I} \cup \{(\boldsymbol{\theta}^{(i)}, \bar{Q}_{HF}^{(i)})\}_{i=N_I+1}^N$, we train a deep network (*DNN*) as a surrogate for the high-fidelity quantity Q_{HF} . We call this surrogate Q_{DNN} ; see Figure 2 (bottom).

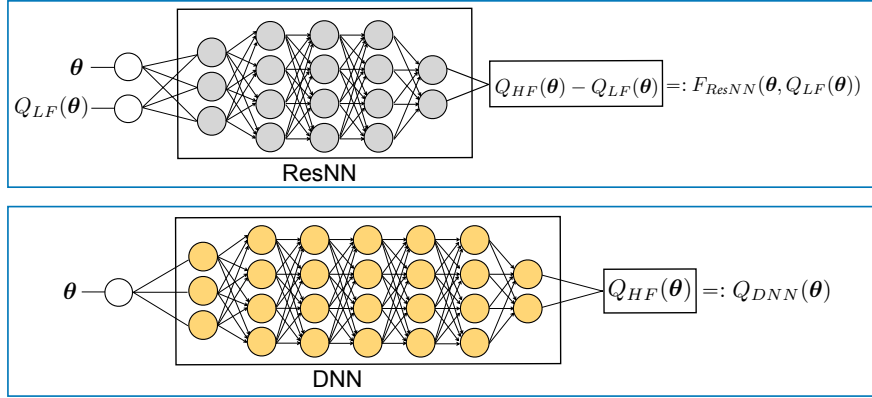


Figure 2: Schematic representation of the RMFNN algorithm, given a set of N low-fidelity and $N_I \ll N$ high-fidelity data. Top: an initial network (*ResNN*) is trained by N_I low-fidelity and high-fidelity data to learn the residual function F . The trained *ResNN* is used along with the rest of $N_{II} = N - N_I$ low-fidelity data to generate a new set of N_{II} high-fidelity data. Bottom: a deep network (*DNN*) is trained by all N high-fidelity data as a surrogate for the high-fidelity target quantity Q_{HF} .

Step 3. Prediction. Given any $\theta \in \Theta$, an approximation $\tilde{Q}(\theta)$ of the target quantity $Q(\theta)$ can be obtained by evaluating the trained deep network *DNN*:

$$\tilde{Q}(\theta) = Q_{DNN}(\theta), \quad \theta \in \Theta. \quad (10)$$

On performance of RMFNN algorithm. Theorem 1 motivates the hypothesis that the RMFNN algorithm will be highly performative when $\|F\|_{L^\infty} \ll \|Q_{HF}\|_{L^\infty}$. Given these conditions, it is important to note that the two networks in the algorithm learn two essentially different quantities: *ResNN* learns the residual function F , while *DNN* learns the target high-fidelity quantity Q_{HF} . Since F has a smaller uniform norm compared to Q_{HF} , *ResNN* can achieve the desired accuracy using a network with fewer degrees of freedom and less training data, relying on a smaller high-fidelity dataset of size N_I . In contrast, *DNN* approximates Q_{HF} , which may require a deeper network and a larger dataset of size N . Importantly, this architectural difference between the two networks pairs well with the training data availability conditions assumed in this and other peer works on multifidelity modeling [20, 21, 22, 23, 24, 25, 26, 27, 28, 29], where the number N_I of available high-fidelity data is small compared to the number N of available low-fidelity data, i.e. $N_I \ll N$. This distinction gives RMFNN an advantage over existing composite algorithms [22, 23], where networks often learn quantities with similar uniform norms and require comparable high-fidelity training data sizes ($N_I \sim N$). By focusing on the residual, RMFNN reduces the reliance on large high-fidelity datasets, improving efficiency in multifidelity modeling.

An alternative approach. We can take a slightly different approach as follows. The first step is the same as in Step 1 above, where we generate low-fidelity and high-fidelity data.

Next, in Step 2, we construct a composite network as follows:

- Using N input-output data $\{(\theta^{(i)}, Q_{LF}^{(i)})\}_{i=1}^N$, we train a deep network (*DNN*) as a surrogate for Q_{LF} .

- Using N_I input data $\{(\boldsymbol{\theta}^{(i)}, Q_{LF}^{(i)})\}_{i=1}^{N_I}$ and N_I output data $\{Q_{HF}^{(i)} - Q_{LF}^{(i)}\}_{i=1}^{N_I}$, we train a second network (*ResNN*) as a surrogate for the residual function F in (4). Note that this part is the same as the first part of step 2 in the original approach, but with a change in the order of implementation.
- We build a composite network by combining *DNN* and *ResNN* as shown in Figure 3.

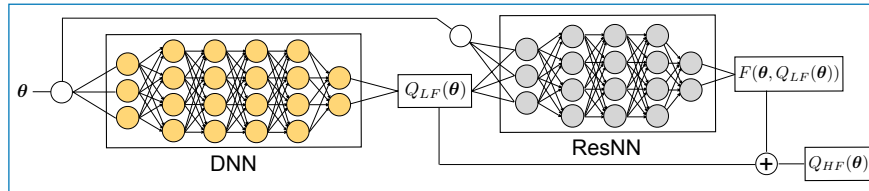


Figure 3: An alternative RMFNN approach. A deep network (*DNN*) is trained using N low-fidelity data to learn Q_{LF} . A second network (*ResNN*) is trained by $N_I \ll N$ low-fidelity and high-fidelity data as a surrogate for the residual F . Finally, the target quantity Q_{HF} is computed by adding Q_{LF} to F .

For prediction in Step 3, given any $\boldsymbol{\theta} \in \Theta$, we compute an approximation $\tilde{Q}(\boldsymbol{\theta})$ of the target quantity $Q(\boldsymbol{\theta})$ by adding the low-fidelity quantity (predicted by *DNN*) to the residual (predicted by *ResNN*); see Figure 3.

A comparison between the two proposed approaches. Both approaches utilize the same residual multi-fidelity formulation (4), but they differ in the way their constituent networks (*ResNN* and *DNN*) work. In the first approach, *ResNN* and *DNN* work at two separate stages: first, *ResNN* learns the residual and generates more high-fidelity data; next, *DNN* uses the initially available and newly generated high-fidelity data to learn the target quantity. In this case, *DNN* alone serves as the surrogate network to be evaluated many times. In the alternative approach, *ResNN* and *DNN* constitute two blocks in a composite surrogate network, and hence both will be evaluated many times. In addition, since in both approaches *ResNN* learns the same residual, and since *DNN* learns either the low- or high-fidelity quantities, which are not expected to be very different in uniform norm, we expect the architectures of *ResNN* and *DNN* to be comparable across both approaches. This gives each approach distinct benefits. When we need many evaluations of the target quantity, the alternative approach may be more expensive, because it requires both *DNN* and *ResNN* to be evaluated, compared to only one evaluation of *DNN* in the first approach. The alternative approach, however, has the flexibility of replacing *DNN* by a direct computation of Q_{LF} , for instance when a direct computation of Q_{LF} is more economical compared to the cost of training and evaluating a network.

Comparison with residual networks. ResNets [32] were originally developed to address the *degradation problem*, a phenomenon where we observe an eventual decrease in network training accuracy as depth increases. ResNets address this problem by introducing shortcut connections that pass along identity maps between layers. In this, as the network depth increases and accuracy becomes saturated, additional layers need only learn a residual that tends to zero as opposed to the full identity map plus some small possibly nonlinear correction. Understood in the context of the recent theoretical results in [13], ResNets take advantage of learning a residual that is small in uniform norm (relative to the identity map) between each layer. It is important to note that the

size of the residual, as formulated in ResNet, is only guaranteed to be small relative to the identity map when the network accuracy is close to saturation and the identity map is near optimal. This situation arises when considering the impact of adding additional layers to a deep neural network that already approximates the quantity of interest to a reasonable accuracy (the conditions of the *degradation* problem). In the context of multi-fidelity modeling, where the map between low-fidelity and high-fidelity models needs to be learned accurately on sparse training data, it is unreasonable to expect the residual between layers (as formulated in ResNet) to be small compared to the identity map. Therefore, in order to take advantage of the previously mentioned theoretical results, we need to explicitly enforce learning a small quantity. This is the exact insight of our proposed RMFNN algorithm. We learn the map between models via a residual function F that targets the discrepancy between high- and low-fidelity models, which in many cases is small in uniform norm.

4 Error and complexity in RMFNN

In this section, we discuss sources of error in the RMFNN algorithm as well as its computational complexity.

4.1 Sources of error

Let ε denote the error (1) in approximating Q by the surrogate (10) obtained by the RMFNN algorithm, measured in L^2 -norm, and satisfying the accuracy constraint

$$\varepsilon = \|Q - Q_{DNN}\|_{L^2(\Theta)} \leq \varepsilon_{TOL}. \quad (11)$$

By triangle inequality, we can split the error into three parts:

$$\varepsilon \leq \underbrace{\|Q - Q_{HF}\|_{L^2(\Theta)}}_{\varepsilon_I} + \underbrace{\|Q_{HF} - \bar{Q}_{HF}\|_{L^2(\Theta)}}_{\varepsilon_{II}} + \underbrace{\|\bar{Q}_{HF} - Q_{DNN}\|_{L^2(\Theta)}}_{\varepsilon_{III}} \leq \varepsilon_{TOL},$$

where the desired accuracy is achieved if, for instance, we enforce $\varepsilon_I, \varepsilon_{II}, \varepsilon_{III} \leq \frac{1}{3} \varepsilon_{TOL}$. The first error term ε_I is the error in approximating Q by Q_{HF} in (8) using an ODE/PDE solver. Then, from (3), it follows that

$$\varepsilon_I \leq C h_{HF}^q,$$

ensuring the accuracy constraint is satisfied by choosing h_{HF} such that $C h_{HF}^q \leq \frac{1}{3} \varepsilon_{TOL}$. The second and third error terms are errors in network approximation, and hence of a different nature. Indeed, the second error term ε_{II} is the error in approximating Q_{HF} by \bar{Q}_{HF} in (9), which is the error in approximating F in (4) by the ResNN surrogate F_{ResNN} ,

$$\varepsilon_{II} = \|Q_{LF} + F - Q_{LF} - F_{ResNN}\|_{L^2(\Theta)} = \|F - F_{ResNN}\|_{L^2(\Theta)}.$$

Similarly, the third error term ε_{III} is the error in approximating \bar{Q}_{HF} by the DNN surrogate Q_{DNN} . Assuming infinite training data, Theorem 1 guarantees the existence of neural networks F_{ResNN} , with depth L_1 and width K_1 , and Q_{DNN} , with depth L_2 and width K_2 , that satisfy the accuracy constraint and have complexity bounds given by

$$\begin{aligned} K_1 L_1^{1/3} &\leq C_1 \|F\|_{L^\infty(\Theta)}^2 \varepsilon_{TOL}^{-2} \log_2^{4/3} \left(\varepsilon_{TOL}^{-1} \right); \\ K_2 L_2^{1/3} &\leq C_2 \|\bar{Q}_{HF}\|_{L^\infty(\Theta)}^2 \varepsilon_{TOL}^{-2} \log_2^{4/3} \left(\varepsilon_{TOL}^{-1} \right). \end{aligned}$$

Importantly, controlling ε_{II} and ε_{III} also depends on our ability to identify the networks F_{ResNN} and Q_{DNN} through a training procedure using finite training data. To the best of the authors’ knowledge, there are currently no neural network training paradigms that establish a rigorous relationship between the achieved tolerance and the quantity and distribution of training data. On the contrary, neural networks are notoriously challenging to train, and the identification of networks that theoretical results, such as Theorem 1, guarantee to exist cannot be assumed; see, for example, [19]. Thus, ε_{II} and ε_{III} should also be viewed as dependent on network training hyperparameters, as well as the quantity and distribution of training data, specifically the choices of the sets Θ_I and Θ_{II} .

Given that the training process is not rigorously understood, the ability to successfully train these networks must be verified numerically. In Section 5, we train all neural networks multiple times using different random seeds and report their variance. This approach aims to provide an empirical understanding of how uncertainty in neural network training manifests within the developed modeling paradigm.

Overall, when F is small in uniform norm, Theorem 1 guarantees the existence of a low-complexity network for which ε_{II} is controlled. We pair this with the hypothesis that the number of training samples required to train a network decreases as its complexity decreases—a relationship we support numerically in Section 5. Together, these motivate the developed modeling paradigm, suggesting that F can be accurately approximated by a low-complexity network trained with a sparse set of both high- and low-fidelity data, which can then be employed to efficiently generate synthetic high-fidelity training data for the network Q_{DNN} .

4.2 Computational complexity

In this section, we address the computational complexity of training and evaluating the networks $ResNN$ and DNN under the accuracy constraint $\varepsilon_{II} + \varepsilon_{III} \leq \frac{2}{3} \varepsilon_{TOL}$. We further emphasize that this work is specifically focused on leveraging neural networks as surrogates for expensive high-fidelity models within query heavy tasks such as uncertainty quantification, where the primary assumption is that evaluating the high-fidelity model represents the dominant cost that needs to be mitigated.

To this end, we discuss the computational complexity of the RMFNN algorithm, denoted as W_{RMFNN} , for approximating the target quantity $Q(\boldsymbol{\theta})$ at $N_{\boldsymbol{\theta}}$ distinct points, particularly when $N_{\boldsymbol{\theta}} \gg 1$ is large.

The complexity of the algorithm comprises two main components: the cost of training the two networks, $ResNN$ and DNN , and the cost associated with evaluations of the deep network estimator given by (10). The training costs for $ResNN$ and DNN can be further broken down into the cost of generating training data and the cost of solving the optimization problem for the network parameters. Since we assume that the evaluations of the high-fidelity model are the primary cost to be reduced, we posit that the cost of training $ResNN$ and DNN is dominated by the expense of obtaining high-fidelity training data. Thus, the dominant cost is assumed to be given by

$$W_{RMFNN} = N_I W_{HF} + N_{\boldsymbol{\theta}} W_{DNN}, \quad (12)$$

where W_{HF} denotes the computational cost of one evaluation of Q_{HF} in (2), and W_{DNN} denotes the cost of one evaluation of DNN . In what follows, we discuss the cost (12) of RMFNN algorithm and compare it, for reference, with the costs associated with the following two approaches:

- HFM: direct sampling of the high-fidelity model without utilizing neural network-based surrogate construction or lower-fidelity information. Here the expensive high-fidelity ODE/PDE model is directly computed N_{θ} times with cost,

$$W_{HFM} = N_{\theta} W_{HF}. \quad (13)$$

- HFNN: evaluation of a deep high-fidelity neural network surrogate that is constructed without leveraging lower-fidelity information. The high-fidelity surrogate network is trained on only N high-fidelity data and evaluated N_{θ} times with cost,

$$W_{HFNN} = N W_{HF} + N_{\theta} W_{DNN}. \quad (14)$$

The higher efficiency of the RMFNN method, compared to the above alternative approaches, relies on the following two conditions:

$$1) N_I \ll N < N_{\theta}; \quad \text{and} \quad 2) W_{DNN} \ll W_{HF}.$$

Clearly, these two conditions imply that $W_{RMFNN} \ll W_{HFNN} < W_{HFM}$. We address each of these conditions in the two observations below.

Observation 1: When $\|F\|_{L^{\infty}} \ll \|Q_{HF}\|_{L^{\infty}}$, Theorem 1 guarantees the existence of networks $ResNN$, approximating F , and DNN , approximating Q_{HF} where for a given tolerance, the complexity of $ResNN$ is considerably less than the complexity of DNN . Given this, we hypothesize that the number N_I of expensive high-fidelity data needed to train $ResNN$ may be far smaller than the total number N of data needed to train DNN , that is $N_I \ll N$. Moreover, in many scientific problems, we often need a very large number ($N_{\theta} \gg 1$) of high-fidelity samples, implying $N < N_{\theta}$. For example, when using Monte Carlo sampling to evaluate the statistical moments of random quantities, we require $N_{\theta} = \mathcal{O}(\varepsilon_{TOL}^{-2})$, since the statistical error in Monte Carlo sampling is known to be proportional to $N_{\theta}^{-1/2}$ [45]. In such cases, the inequality $N < N_{\theta}$ holds provided $N = \mathcal{O}(\varepsilon_{TOL}^{-p})$, with $p < 2$. We note that there are currently no rigorous results that relate the number and distribution of input training data to the accuracy of deep neural networks. However, we have observed through numerical experiments that for the type and size of networks that we have studied, the number of data needed to train a network to achieve accuracy within ε_{TOL} indeed grows with a rate milder than $\mathcal{O}(\varepsilon_{TOL}^{-2})$.

Observation 2: The evaluation of a neural network mainly involves simple matrix-vector multiplications and evaluations of activation functions. The total evaluation cost depends on the width and depth of the network and the type of activation used. Crucially, the network evaluation cost depends only mildly on the complexity of the underlying ODE/PDE problem. As can be seen in Theorem 1, approximating target functions with successively lower regularity or larger problem input dimension will require neural networks of higher complexity (larger width and/or depth). However, when evaluating the neural network, this added complexity manifests only as additional simple matrix-vector operations and cheap evaluations of activation functions. In particular, for QoIs that can be well approximated by a network with several hidden layers and hundreds or thousands of neurons, we expect $W_{ResNN} < W_{DNN} \ll W_{HF}$. Indeed, in such cases, the more complex the high-fidelity problem, and the more expensive computing the high-fidelity quantity, the smaller the ratio W_{DNN}/W_{HF} .

It is to be noted that in the above discussion we have assumed that the cost of training DNN is dominated by the cost of obtaining high-fidelity training data, neglecting the one-time cost of solving

the underlying optimization problem in the training process. This will be a valid assumption, for instance, when the cost of solving the network optimization problem (e.g. by stochastic gradient descent) is negligible compared to the cost of $N \gg 1$ high-fidelity model evaluations. In particular, we have observed through numerical experiments that as the tolerance decreases, and hence N increases, this one-time network training cost may become negligible compared to the cost of N high-fidelity solves. We further illustrate this in Section 5.

An illustrative example. We compare the costs (12), (13), and (14) on a prototypical UQ task. Let $\boldsymbol{\theta}$ be a random vector with a known and compactly supported joint probability density function (PDF), and suppose that we want to obtain an accurate expectation of the random quantity $Q = Q(\boldsymbol{\theta})$ within a small tolerance, $\varepsilon_{TOL} \ll 1$. To achieve this using MC sampling, recalling that the statistical error in MC sampling is proportional to $N_{\boldsymbol{\theta}}^{-1/2}$ [45], we require $N_{\boldsymbol{\theta}} \propto \varepsilon_{TOL}^{-2} \gg 1$ samples. Now, suppose that $W_{HF} \propto h_{HF}^{-\gamma}$, where $\gamma > 0$ is related to the time-space dimension of the underlying ODE/PDE problem and the discretization technique used to solve the problem. Then, noting $h_{HF} \propto \varepsilon_{TOL}^{1/q}$, we obtain $W_{HF} \propto \varepsilon_{TOL}^{-\gamma/q}$. Therefore, the cost (13) of directly computing the high-fidelity model $N_{\boldsymbol{\theta}}$ times is

$$W_{HF} \propto \varepsilon_{TOL}^{-(2+\gamma/q)}. \quad (15)$$

Following observation 1 above, we assume $N \propto \varepsilon_{TOL}^{-p}$, with $p < 2$. This assumption indicates that the dependence of number N of training data on the tolerance ε_{TOL} is milder than the dependence of number of MC samples on the tolerance. Furthermore, we assume $r := N_I/N \ll 1$. Finally, following observation 2 above, we assume that the evaluation cost of the deep network DNN is less than the cost of a high-fidelity solve, i.e. $W_{DNN} \propto \varepsilon_{TOL}^{-\hat{p}}$, with $\hat{p} < \gamma/q$, implying $W_{DNN} \ll W_{HF}$. With these assumptions, the cost (14) of using a purely high-fidelity network surrogate and the cost (12) of using a surrogate generated by the RMFNN algorithm read

$$W_{HFNN} \propto \varepsilon_{TOL}^{-(p+\gamma/q)} + \varepsilon_{TOL}^{-(2+\hat{p})} + \text{training cost}, \quad (16)$$

$$W_{RMFNN} \propto r \varepsilon_{TOL}^{-(p+\gamma/q)} + \varepsilon_{TOL}^{-(2+\hat{p})} + \text{training cost}. \quad (17)$$

Comparing (15) and (16), and excluding training costs (see the discussion above), we get $W_{HFNN} \ll W_{HF}$, when $p < 2$ and $\hat{p} < \gamma/q$. Furthermore, comparing (16) and (17), we get $W_{RMFNN} \ll W_{HFNN}$, when $r \ll 1$ and $\hat{p} < p + \gamma/q - 2$.

5 Numerical examples

In this section, we apply the proposed RMFNN algorithm to four numerical examples. The first one provides a focused numerical justification for the residual formulation present in the RMFNN algorithm, and the remaining examples comprise parametric ODE/PDE problems, of which the latter two are borrowed from [23]. In all problems, the parameters are represented by a d -dimensional random vector $\boldsymbol{\theta} \in \Theta \subset \mathbb{R}^d$, with a known and bounded joint PDF, $\pi : \Theta \rightarrow \mathbb{R}_+$. For each parametric problem, we consider a desired output quantity $Q : \Theta \rightarrow \mathbb{R}$, being a functional of the ODE/PDE solution. Our goal is to compute an accurate and efficient surrogate for Q , denoted by Q_{DNN} , given by (10). We will measure the approximation error using the weighted L^2 -norm, as defined in (1) with $p = 2$. We approximate the error by sample averaging, using N_{ε} independent samples $\{\boldsymbol{\theta}^{(i)}\}_{i=1}^{N_{\varepsilon}} \in \Theta$ drawn from $\pi(\boldsymbol{\theta})$, and record the weighted mean squared error (MSE),

$$\varepsilon = \int_{\Theta} |Q(\boldsymbol{\theta}) - Q_{DNN}(\boldsymbol{\theta})|^2 \pi(\boldsymbol{\theta}) d\boldsymbol{\theta} \approx \frac{1}{N_{\varepsilon}} \sum_{i=1}^{N_{\varepsilon}} |Q(\boldsymbol{\theta}^{(i)}) - Q_{DNN}(\boldsymbol{\theta}^{(i)})|^2 =: \varepsilon_{MSE}. \quad (18)$$

To facilitate a comparison of our algorithm with that of [23], two of our numerical examples involve computing the expectation of Q ,

$$\mathbb{E}[Q] := \int_{\Theta} Q(\boldsymbol{\theta}) \pi(\boldsymbol{\theta}) d\boldsymbol{\theta},$$

by MC sampling. Due to the slow convergence of MC sampling, obtaining an accurate estimation may require a very large number ($N_{\boldsymbol{\theta}} \gg 1$) of realizations of Q , each of which requires an expensive high-fidelity ODE/PDE solve. We will approximate all $N_{\boldsymbol{\theta}}$ realizations of Q by the proposed surrogate Q_{DNN} , built on far less than $N_{\boldsymbol{\theta}}$ number of ODE/PDE solves. This is an exemplary setting where we need many evaluations of Q_{DNN} . To this end, we generate $N_{\boldsymbol{\theta}}$ independent samples of $\boldsymbol{\theta}$, say $\{\boldsymbol{\theta}^{(i)}\}_{i=1}^{N_{\boldsymbol{\theta}}}$, according to the joint PDF $\pi(\boldsymbol{\theta})$ and approximate $\mathbb{E}[Q]$ by the sample mean of its approximated realizations computed by the RMFNN algorithm:

$$\mathbb{E}[Q] \approx \mathcal{A}_{RMFNN} := \frac{1}{N_{\boldsymbol{\theta}}} \sum_{i=1}^{N_{\boldsymbol{\theta}}} Q_{DNN}(\boldsymbol{\theta}^{(i)}). \quad (19)$$

We compare the complexity of (19) with that of a direct high-fidelity MC computation,

$$\mathbb{E}[Q] \approx \mathcal{A}_{HF} := \frac{1}{N_{\boldsymbol{\theta}}} \sum_{i=1}^{N_{\boldsymbol{\theta}}} Q_{HF}(\boldsymbol{\theta}^{(i)}). \quad (20)$$

In addition to the mean squared error (18), we also report the absolute and relative errors in expectations,

$$\varepsilon_{abs} := |\mathbb{E}[Q(\boldsymbol{\theta})] - \mathcal{A}|, \quad \varepsilon_{rel} := |\mathbb{E}[Q(\boldsymbol{\theta})] - \mathcal{A}| / |\mathbb{E}[Q(\boldsymbol{\theta})]|, \quad (21)$$

where the estimator \mathcal{A} is either \mathcal{A}_{RMFNN} or \mathcal{A}_{HF} . We note that ε_{abs} and ε_{rel} contain both the deterministic error (due to approximating Q by either Q_{DNN} or Q_{HF}) and the statistical error (due to MC sampling of Q_{DNN} or Q_{HF}). In the case of approximation Q by Q_{DNN} , we can employ triangle inequality and write

$$\varepsilon_{abs} \leq |\mathbb{E}[Q(\boldsymbol{\theta}) - Q_{DNN}(\boldsymbol{\theta})]| + |\mathbb{E}[Q_{DNN}(\boldsymbol{\theta})] - \mathcal{A}_{RMFNN}|,$$

where the first (deterministic) term is indeed the error measured in the weighted L^1 -norm, as given in (1) with $p = 1$.

In all examples the closed-form solutions to the problems, and hence the true values of $Q(\boldsymbol{\theta})$, are known. We use these closed-form solutions to compute errors in the approximations, and we always compare the cost of different methods subject to the same accuracy constraint. All codes are written in Python and run on a single CPU. To construct neural networks we leverage Pytorch [46] in examples 5.1 and 5.2, and Keras [47] in examples 5.3 and 5.4, both of which are open-source neural-network libraries written in Python. It is to be noted that all CPU times are measured by `time.process_time()` in Python, taking average of tens of simulations.

5.1 A comparison of residual formulations

While formulation (4) represents the residual as a function of both θ and Q_{LF} , it can alternatively be expressed solely in terms of θ , isolating it from Q_{LF} . This leads to an alternative framework, referred to here as the Discrepancy Neural Network (DiscrepNN), which models the difference between the low- and high-fidelity outputs as a function of θ . In this example, we compare the performance of these two frameworks, where:

1. RMFNN learns: $F(\theta, Q_{LF}(\theta)) = Q_{HF}(\theta) - Q_{LF}(\theta)$,
2. DiscrepNN learns: $G(\theta) = Q_{HF}(\theta) - Q_{LF}(\theta)$.

Consider high- and low-fidelity models defined by

$$Q_{LF}(\theta) = |0.5 \sin(8\pi(\theta + 1))| \quad Q_{HF}(\theta) = 2(1 + 0.2\theta)Q_{LF}(\theta)^{1.5}, \quad \theta \in [0, 1]. \quad (22)$$

In Figure 4, we plot the residual function G (left), and the residual function F (right).

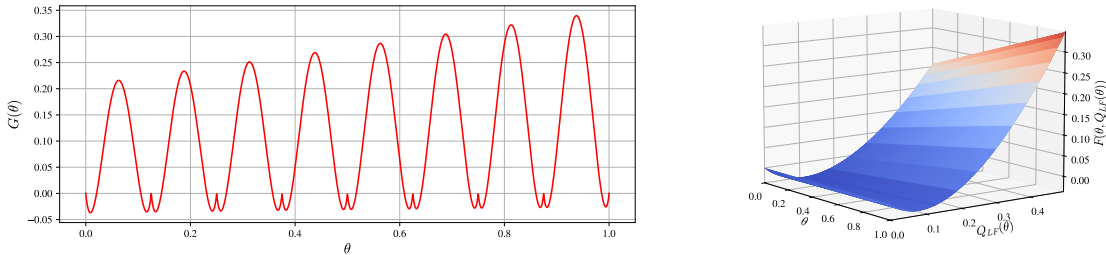


Figure 4: Two different residual functions: on the left $G(\theta)$, and on the right $F(\theta, Q_{LF}(\theta))$

Note that while the input dimension of F is one higher than that of G , F is characterized by low frequency and a more regular profile. We hypothesize that this allows F to be learned from sparser training data compared to G . To test this, we compare the approximation of F and G using neural networks under varying data sparsity conditions. Across both the RMFNN and DiscrepNN, we use a fixed neural network architecture consisting of $L = 2$ layers and $K = 10$ neurons per layer. Moreover, all ReLU networks are constructed with a ResNet-style architecture, where we implement shortcut connections that pass along the identity map every two layers. We remark here that Theorem 1 also holds for ReLU ResNets. This is shown in [13], where a strategy is developed to re-parameterize ReLU ResNets into standard ReLU networks with marginal change in network complexity. For each method, the networks are trained on twelve different training sets where the number of high-fidelity (and low-fidelity) training samples ranges from 4 to 48. These training sets are generated using a random uniform distribution over the parameter space. Moreover, the training sample inputs and outputs are normalized so that they reside in $[0, 1] \times [0, 1]$. For training, we use the Adam optimization algorithm with the MSE cost function and Tikhonov regularization, and we implement an adaptive learning rate and stop criterion by monitoring the MSE on a validation set. To account for the randomness inherent in the training process, for each training set and for each surrogate method, we train and test 20 separate times on 20 distinct random seeds. From each train/test trial we compute the MSE (18) in the surrogate prediction on an independent test set of $N_\varepsilon = 10^6$ points θ uniformly distributed in $[0, 1]$. Figure 5 displays MSE versus the number of high-fidelity samples in the training set over 20 different training runs on distinct random seeds. The larger markers with bold outline indicate the average MSE over each ensemble.

In examining the sparsest training dataset (comprising only 4 samples), both the RMFNN and DiscrepNN exhibit similarly poor performance characterized by an average MSE around 10^{-1} and

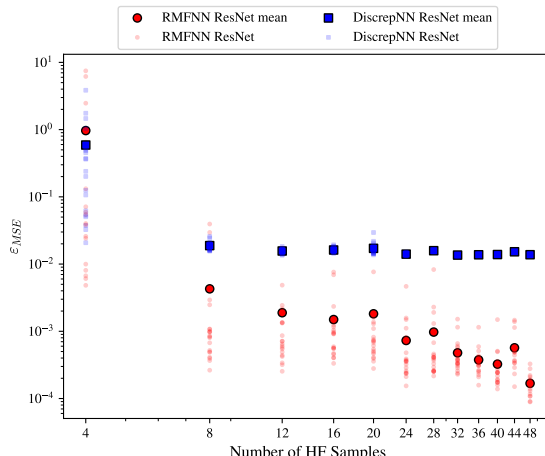


Figure 5: Mean squared error ε_{MSE} over 20 training runs approximating $Q_{HF}(\theta) - Q_{LF}(\theta)$ by RMFNN ResNet (red), and DiscrepNN ResNet (blue); average MSE over each ensemble is indicated by the larger marker with bold outline

very high variance. This outcome is not surprising; with such limited data, it would be unexpected for either network to produce a high-quality surrogate. For the other datasets, the RMFNN consistently demonstrates a significantly lower average MSE compared to the DiscrepNN, suggesting that formulating the residual function as $F(\theta, Q_{LF}(\theta))$ is advantageous compared to the formulation $G(\theta)$. While the variance in the MSE for the RMFNN is generally higher than that of the DiscrepNN, it is noteworthy that this variability tends to favor predictions with a squared approximation error lower than the average across the ensemble. As the number of training samples increases, the average MSE for the DiscrepNN plateaus around 10^{-2} , whereas the RMFNN’s MSE continues to decrease, reaching nearly two orders of magnitude smaller at around 10^{-4} . This performance discrepancy, coupled with the higher frequency content of the function G compared to the function F , suggests that the DiscrepNN may require a more complex network architecture to further reduce MSE. This reinforces the importance of the residual formulation $F(\theta, Q_{LF}(\theta))$; within the RMFNN framework, the residual function can be effectively approximated by a low-complexity network capable of learning from sparse data. Overall, this example illustrates how incorporating low-fidelity model outputs into the residual function’s input space can simplify the target function’s profile, allowing it to be learned by a less complex network, even with limited training data.

5.2 The impact of a small residual uniform norm

In this numerical experiment, we perform a surrogate construction task using bi-fidelity information, highlighting the advantage of approximating a residual function with small uniform norm. We consider a pulsed harmonic oscillator governed by the system of ODEs,

$$\dot{\mathbf{u}}(t) = A \mathbf{u}(t) + \cos(\omega t) \mathbf{b}, \quad \mathbf{u} = \begin{bmatrix} u_1 \\ u_2 \end{bmatrix}, \quad A = \begin{bmatrix} -2 & 0 \\ 0 & -0.25 \end{bmatrix}, \quad \mathbf{b} = \begin{bmatrix} b_1 \\ b_2 \end{bmatrix}, \quad (23)$$

with initial solution $\mathbf{u}(0) = (1, 20)^\top$. We consider four model parameters: the frequency $\omega \in [5, 50]$, the oscillation time $t \in [0, 6]$, and two pulse parameters $(b_1, b_2) \in [0, 0.2] \times [4, 4.5]$, forming a four-dimensional parameter vector $\boldsymbol{\theta} = (\omega, t, b_1, b_2)$. Our goal is to construct a surrogate for the kinetic

energy of the system,

$$Q(\boldsymbol{\theta}) = \|\mathbf{u}(\boldsymbol{\theta})\|_2 = (u_1^2(\boldsymbol{\theta}) + u_2^2(\boldsymbol{\theta}))^{1/2}, \quad \boldsymbol{\theta} = (\omega, t, b_1, b_2).$$

To this end, we utilize multi-fidelity modeling as follows. For the high-fidelity model Q_{HF} we leverage the exact analytic solution to (23), and for the low-fidelity model Q_{LF} we employ an asymptotic method (see [43] and section 3.1) to derive a closed form asymptotic approximation. In Figure 6, the residual $F = Q_{HF} - Q_{LF}$ and the high-fidelity quantity Q_{HF} are plotted for $b_1 = 0.2$ and $b_2 = 4.5$. Notice that both Q_{HF} and F are of similar oscillatory character, but

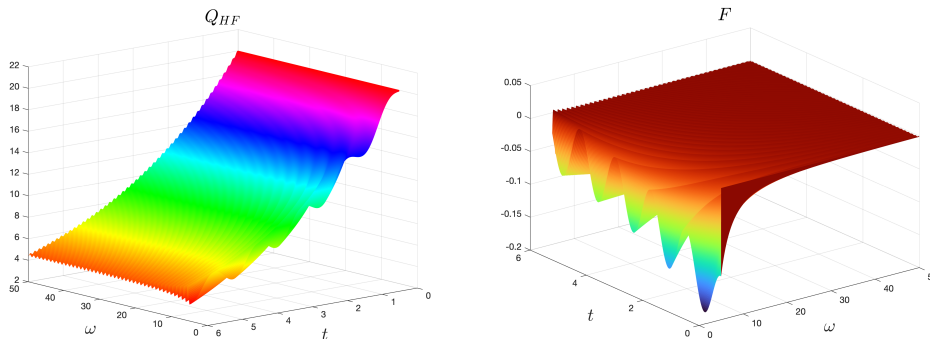


Figure 6: Profiles of Q_{HF} (left) and F (right) versus (ω, t) for $b_1 = 0.2$ and $b_2 = 4.5$.

$\|F\|_\infty \ll \|Q_{HF}\|_\infty$. Thus based on the discussion of Theorem 1 in Section 3.1, we expect the RMFNN algorithm to be performative with the largest advantage under conditions of sparse training data. We will compare three different methods:

1. RMFNN ResNet: our proposed residual multi-fidelity algorithm using ReLU ResNets.
2. MFNN ResNet: the multi-fidelity framework proposed in [23] using ReLU ResNets;
3. HFNN ResNet: a single-fidelity ReLU ResNet trained on only high-fidelity data.

For the RMFNN algorithm we employ the alternative approach discussed in section 3.2, and, further, we replace the training of the deep network DNN by direct evaluations of the low-fidelity model. As such, each of the three surrogate methods requires the training of just one neural network. For clarity, we state the mapping that each of the methods learns below:

- RMFNN learns: $(\boldsymbol{\theta}, Q_{LF}(\boldsymbol{\theta})) \mapsto (Q_{HF}(\boldsymbol{\theta}) - Q_{LF}(\boldsymbol{\theta}))$
- MFNN learns: $(\boldsymbol{\theta}, Q_{LF}(\boldsymbol{\theta})) \mapsto Q_{HF}(\boldsymbol{\theta})$
- HFNN learns: $\boldsymbol{\theta} \mapsto Q_{HF}(\boldsymbol{\theta})$

Across all three methods we use a fixed ReLU network architecture consisting of $L = 7$ layers, $K = 7$ neurons in each hidden layer, and one ReLU-free neuron in the last layer. Moreover, to facilitate a comparison of our residual multi-fidelity framework with standard ResNets [32], all ReLU networks are constructed with a ResNet-style architecture, where we implement shortcut connections that pass along the identity map every two layers. For each method, ReLU networks are trained on eleven different training sets where the number of high-fidelity (and low-fidelity)

training samples ranges from 250 to 17000. These training sets are generated using a multi-variate uniform distribution over the parameter space. Moreover, the training sample inputs and outputs are normalized so that they reside in $[0, 1]^4 \times [0, 1]$. For training, we use the Adam optimization algorithm with the MSE cost function and Tikhonov regularization. We implement an adaptive learning rate and stop criterion by monitoring the MSE on a validation set. To account for the randomness inherent in the training process, we train and test each surrogate method 20 separate times using distinct random seeds for each training set. From each train/test trial, we compute the MSE (18) in the surrogate prediction, evaluated on an independent test set of $N_\varepsilon = 10^6$ points θ uniformly distributed in Θ . Figure 7 displays MSE versus the number of high-fidelity samples in the training set over 20 different training runs on distinct random seeds. The larger markers with bold outline indicate the average MSE over each ensemble.

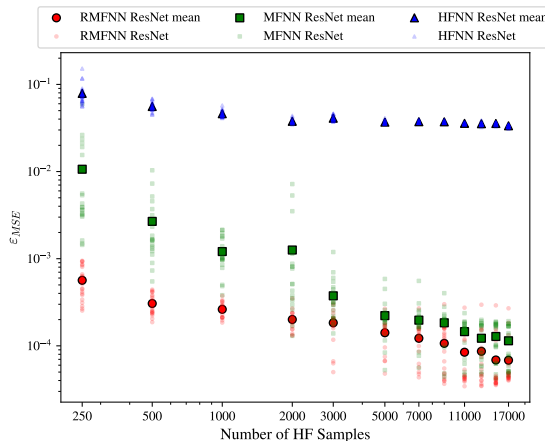


Figure 7: Mean squared error ε_{MSE} over 20 training runs approximating Q_{HF} by HFNN ResNet (blue), MFNN ResNet (green) and RMFNN ResNet (red) versus number of high-fidelity training samples; average MSE over each ensemble is indicated by the larger marker with bold outline

As shown in Figure 7, RMFNN consistently outperforms the other methods in terms of average MSE across the ensemble, with the performance advantage being most pronounced under sparse training data—the exact conditions desired in multi-fidelity computation. These results underscore the importance of incorporating both key principles that motivate the RMFNN algorithm:

- (i) *Leveraging potentially non-linear correlations between low-fidelity and high-fidelity models.*
- (ii) *Ensuring the quantity learned during network training is small in uniform norm compared to the high-fidelity quantity of interest.*

Table 1 summarizes the three surrogate methods in the context of properties (i) and (ii). A check mark (\checkmark) indicates that the method satisfies the corresponding property.

Property (i) is harnessed by both RMFNN and MFNN, and the orders of magnitude reduction in mean squared error for the MFNN method over the HFNN method verifies its importance. Property (ii), on the other hand, is unique to RMFNN. The additional reduction in mean squared error achieved by RMFNN over MFNN validates the benefit of learning a quantity with a small uniform norm relative to the high-fidelity output.

The orders of magnitude reduction in error for the RMFNN ResNet over the HFNN ResNet also shows that our residual multi-fidelity framework makes a meaningful improvement over simply

methods	(i)	(ii)
HFNN		
MFNN	✓	
RMFNN	✓	✓

Table 1: Comparison of RMFNN, MFNN, and HFNN methods in the context of properties (i) and (ii)

using ResNet-style shortcut connections in a single-fidelity network. In particular, these results support our discussion in Section 3.2, where we compare the residual formulation in ResNet [32] with our residual multi-fidelity framework.

Examining the spread in MSE across different random seeds used for training, we observe significantly higher variance in the MFNN compared to the RMFNN in the sparse data regime. For the HFNN and MFNN, the variance decreases as the number of high-fidelity training samples increases. In contrast, the variance in the RMFNN appears to increase slightly with larger training sets. Importantly, for more plentiful data, the variability in RMFNN predictions is biased towards MSE values smaller than the ensemble average, highlighting its robustness in performance.

We remark that while the results in Figure 7 were obtained for a fixed network architecture with $(K, L) = (7, 7)$, the experiment was also conducted for $(K, L) = (25, 7)$ and $(K, L) = (7, 15)$. The results obtained for these different network architectures are analogous to those pictured in Figure 7 up to a universal and commensurate reduction in MSE across all surrogate methods. Such a reduction in error can be explained by an increase in the number of trainable parameters and hence in the expressive capacity of the networks.

5.3 A parametric ODE problem

Consider the following parametric initial value problem (IVP),

$$\begin{aligned} u_t(t, \theta) + 0.5 u(t, \theta) &= f(t, \theta), & t \in [0, T], \\ u(0, \theta) &= g(\theta), \end{aligned} \tag{24}$$

where $\theta \in \Theta = [-1, 1]$ is a uniformly distributed random variable. Using the method of manufactured solutions, we choose the force term f and the initial data g so that the exact solution to the IVP (24) is

$$u(t, \theta) = 0.5 + 2 \sin(12\theta) + 6 \sin(2t) \sin(10\theta)(1 + 2\theta^2).$$

Now consider the target quantity

$$Q(\theta) = u(T, \theta), \quad T = 100.$$

Our goal is to utilize the RMFNN algorithm to construct a surrogate Q_{DNN} for Q , which will then be used to perform MC sampling to estimate the expectation $\mathbb{E}[Q(\theta)]$.

Multi-fidelity models and accuracy constraint. Suppose that we use the second-order accurate Runge-Kutta (RK2) time-stepper as the deterministic solver to compute realizations of $Q_{LF}(\theta)$ and $Q_{HF}(\theta)$ using time steps h_{LF} and h_{HF} , respectively. We perform a simple error analysis, similar to the analysis in [23], to obtain the minimum number of realizations N_θ and the maximum time step h_{HF} for the high-fidelity model to satisfy the accuracy constraint $\varepsilon_{rel} \leq \varepsilon_{TOL}$ with a 1% failure

probability, i.e. $\text{Prob}(\varepsilon_{rel} \leq \varepsilon_{TOL}) = 0.99$. Here ε_{rel} is the relative error given in (21). Table 2 summarizes the numerical parameters (N_θ, h_{HF}, h_{LF}) and the CPU time of evaluating single realizations of Q_{LF} and Q_{HF} for a decreasing sequence of tolerances $\varepsilon_{TOL} = 10^{-2}, 10^{-3}, 10^{-4}$. We choose $h_{LF} = s h_{HF}$, with $s = 5, 10, 10$, for the three tolerance levels.

Table 2: Required number of realizations and time steps to achieve $\text{P}(\varepsilon_{rel} \leq \varepsilon_{TOL}) = 0.99$.

ε_{TOL}	N_θ	h_{HF}	W_{HF}	h_{LF}	W_{LF}
10^{-2}	1.35×10^5	0.1	1.99×10^{-4}	0.5	3.99×10^{-5}
10^{-3}	1.35×10^7	0.025	8.36×10^{-4}	0.25	8.35×10^{-5}
10^{-4}	1.35×10^9	0.01	2.39×10^{-3}	0.1	2.39×10^{-4}

Surrogate construction. Following the algorithm in Section 3.2, we first generate a set of $N = N_I + N_{II}$ points, $\theta^{(i)} \in [-1, 1]$, with $i = 1, \dots, N$, collected into two disjoint sets, Θ_I and Θ_{II} . We choose the points to be uniformly placed on the interval $[-1, 1]$. We select every 10th point to be in the set Θ_I , and we collect the rest of the points in the set Θ_{II} . This implies $N \approx 10 N_I$, meaning that we need to compute the target quantity $Q(\theta)$ by the high-fidelity model (using RK2 with time step h_{HF}) at only 10% of points, i.e. $r = N_I/N \approx 0.1$; compare this with $r = 0.25$ taken in [23] to achieve the same accuracy. The number of points N will be chosen based on the desired tolerance, slightly increasing as the tolerance decreases, i.e. $N \propto \varepsilon_{TOL}^{-p}$ where $p > 0$ is small. In particular, we observe in Table 3 below that the value $p = 0.5$ is enough to meet our accuracy constraints.

The architecture of *ResNN* consists of 2 hidden layers, where each layer has 10 neurons. The architecture of *DNN* consists of 4 hidden layers, where each layer has 20 neurons. The architecture of both networks will be kept fixed at all tolerance levels. For the training process, we employ the MSE cost function and use Adam optimization technique. For both networks, we split the available data points into a training set (95% of data) and a validation set (5% of data) and adaptively tune the learning rate parameter. We do not use any regularization technique. Moreover, in order to take into account the uncertainty inherent in neural network training, each neural network is trained five separate times on five different random seeds. Table 3 summarizes the number of training-validation data N_I (for *ResNN*) and N (for *DNN*), the number of epochs N_{epoch} , batch size N_{batch} , and the average CPU time of training and evaluating the two networks for different tolerances over the five independent training trials. We remark that the variance in training and evaluation time is negligible across the different trials. With these parameters we construct three surrogates for Q_{DNN} , one at each tolerance level. We note that while using a different architecture and other choices of network parameters (e.g. number of layers/neurons and learning rates) may give more efficient networks, the selected architectures and parameters here, following the general guidelines in [48, 49], produce satisfactory results in terms of efficiency and accuracy; see Table 4 and Figures 8-10 below.

Table 3: The number of training data and average training and evaluation time of the two networks.

ε_{TOL}	N_I	N	<i>ResNN</i> : 2×10 neurons				<i>DNN</i> : 4×20 neurons			
			N_{epoch}	N_{batch}	W_{T_1}	W_{P_1}	N_{epoch}	N_{batch}	W_{T_2}	W_{P_2}
10^{-2}	25	241	100	10	5.19	2.10×10^{-5}	400	40	20.40	2.80×10^{-5}
10^{-3}	81	801	1500	30	70.08	2.10×10^{-5}	8000	80	446.39	2.80×10^{-5}
10^{-4}	321	3201	5000	50	276.86	2.10×10^{-5}	20000	200	1378.82	2.80×10^{-5}

Table 4 reports the MSE (18) in the constructed surrogates Q_{DNN} using $N_\varepsilon = 10^6$ evenly distributed points θ in Θ , confirming that the (deterministic) MSE in the network approximation is comparable to the (statistical) relative error ε_{rel} over all five training runs.

Table 4: MSE in the approximation $Q_{DNN}(\theta) \approx Q(\theta)$.

ε_{TOL}	10^{-2}	10^{-3}	10^{-4}
ε_{MSE} (Trial 1)	6.98×10^{-2}	4.87×10^{-3}	2.08×10^{-4}
ε_{MSE} (Trial 2)	3.13×10^{-2}	5.71×10^{-3}	1.37×10^{-4}
ε_{MSE} (Trial 3)	5.10×10^{-2}	7.66×10^{-3}	2.95×10^{-4}
ε_{MSE} (Trial 4)	9.10×10^{-2}	5.50×10^{-3}	1.97×10^{-4}
ε_{MSE} (Trial 5)	1.14×10^{-2}	1.38×10^{-3}	1.95×10^{-4}

Figure 8 shows the low-fidelity and high-fidelity quantities versus $\theta \in [-1, 1]$ (solid lines) and the data (circle and triangle markers) available in the case $\varepsilon_{TOL} = 10^{-2}$. Figure 9 (left) shows the pointwise mean of the generated high-fidelity data by the network *ResNN* over all five training runs together with 2 standard deviations. The variance in the generated data is very small, barely visible in the plot, owing to the fact that *ResNN* predicts a quantity that is very small in uniform norm relative to the high-fidelity QoI. Figure 9 (right) shows the pointwise mean predicted high-fidelity quantity by the deep network *DNN* together with 2 standard deviations over the five independent training runs.

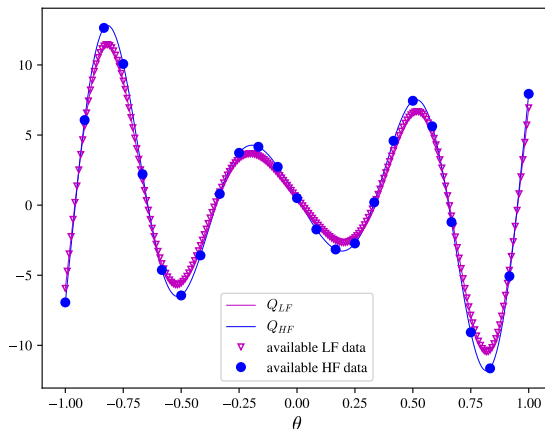


Figure 8: The low-fidelity and high-fidelity quantities versus $\theta \in [-1, 1]$ (solid lines) and the available data (markers) in the case $\varepsilon_{TOL} = 10^{-2}$. There are $N_I = 25$ high-fidelity and $N = 241$ low-fidelity data points, represented by circles and triangles, respectively.

MC sampling. We next compute $\mathbb{E}[Q]$ by (19) and (20) and compare their complexities. Figure 10 (left) shows the CPU time as a function of tolerance. The computational cost of a direct high-fidelity MC computation (20) is $\mathcal{O}(\varepsilon_{TOL}^{-2.5})$, following (15) and noting that the order of accuracy of RK2 is $q = 2$, and that the time-space dimension of the problem is $\gamma = 1$. On the other hand, if we only consider the prediction time of the proposed residual multi-fidelity method, excluding the training

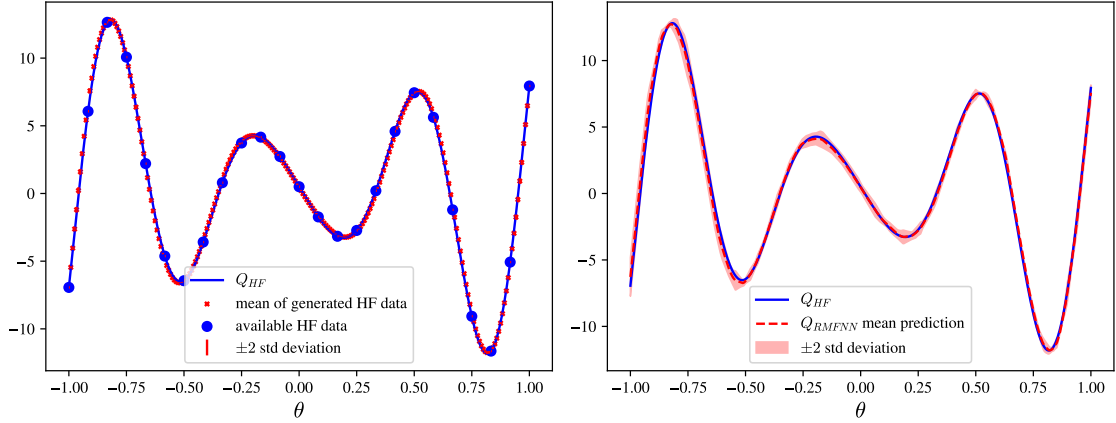


Figure 9: Outputs of the trained networks for $\varepsilon_{TOL} = 10^{-2}$. Left: generated data by the network, *ResNN*. Right: predicted quantity by the deep network, *DNN*.

costs, the cost is $\mathcal{O}(\varepsilon_{TOL}^{-2})$, which is much less than the cost of high-fidelity MC sampling. When adding the training costs, we observe that although for large tolerances the training cost is large, as the tolerance decreases, the training costs become negligible compared to the total CPU time. Overall, the cost of the proposed method approaches $\mathcal{O}(\varepsilon_{TOL}^{-2})$ as tolerance decreases, and hence, the smaller the tolerance, the more gain in computational cost when employing the proposed method over high-fidelity MC sampling. This can also be seen by (17) noting that $\max(p + \gamma/q, 2 + \hat{p}) = \max(0.5 + 0.5, 2 + \hat{p},) = 2 + \hat{p}$, where $\hat{p} > 0$ is very small. We note that while we observe significant cost reductions at the tested tolerances, training neural networks to achieve very small tolerances can be challenging, and what is required to do this in practice, be it additional training data or optimization time is not rigorously understood [19]. Therefore, we do not assert that the demonstrated scaling will necessarily apply in these extremely small tolerance scenarios. Finally, Figure 10 (right) shows 20 instances of the relative error as a function of tolerance computed as 4 Monte Carlo simulations from each of the 5 independent network training runs. We see considerable variance in the network performance across different training runs, but even taking this variance into account, we meet the desired tolerance across all simulations.

5.4 A parametric PDE problem

Consider the following parametric initial-boundary value problem (IBVP)

$$\begin{aligned}
 u_{tt}(t, \mathbf{x}, \boldsymbol{\theta}) - \Delta_{\mathbf{x}} u(t, \mathbf{x}, \boldsymbol{\theta}) &= f(t, \mathbf{x}, \boldsymbol{\theta}), & (t, \mathbf{x}, \boldsymbol{\theta}) &\in [0, T] \times D \times \Theta, \\
 u(0, \mathbf{x}, \boldsymbol{\theta}) &= g_1(\mathbf{x}, \boldsymbol{\theta}), \quad u_t(0, \mathbf{x}, \boldsymbol{\theta}) = g_2(\mathbf{x}, \boldsymbol{\theta}), & (t, \mathbf{x}, \boldsymbol{\theta}) &\in \{0\} \times D \times \Theta, \\
 u(t, \mathbf{x}, \boldsymbol{\theta}) &= g_b(t, \mathbf{x}, \boldsymbol{\theta}), & (t, \mathbf{x}, \boldsymbol{\theta}) &\in [0, T] \times \partial D \times \Theta,
 \end{aligned} \tag{25}$$

where $t \in [0, T]$ is the time, $\mathbf{x} = (x_1, x_2) \in D$ is the vector of spatial variables in a square domain $D = [-1, 1]^2$, and $\boldsymbol{\theta} = (\theta_1, \theta_2) \in \Theta$ is a vector of two independently and uniformly distributed random variables on $\Theta = [10, 11] \times [4, 6]$. We select the force term f and the initial-boundary data g_1, g_2, g_b so that the exact solution to the IBVP (25) is

$$u(t, \mathbf{x}, \boldsymbol{\theta}) = \sin(\theta_1 t - \theta_2 x_1) \sin(\theta_2 x_2).$$

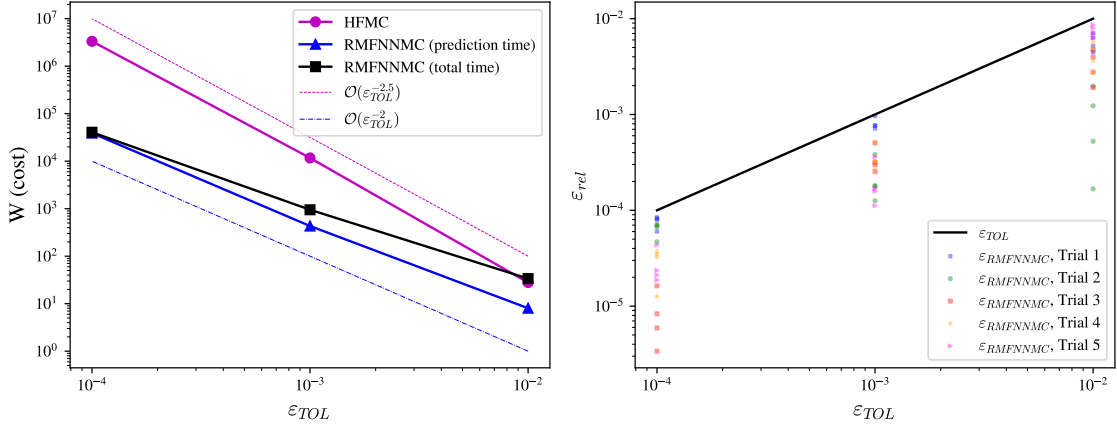


Figure 10: CPU time and error versus tolerance. Left: for large tolerances the training cost is dominant, making the cost of RMFNNMC comparable to the cost of HFMC. However, as tolerance decreases, the training cost becomes negligible and the cost of RMFNNMC approaches $\mathcal{O}(\epsilon_{TOL}^{-2})$; Right: relative error over different training trials as a function of tolerance verifies that the tolerance is met with 1% failure probability; different markers indicate 4 Monte Carlo simulations from each training trial

We consider the target quantity,

$$Q(\boldsymbol{\theta}) = u(T, \mathbf{x}_Q, \boldsymbol{\theta}), \quad T = 30, \quad \mathbf{x}_Q = (0.5, 0.5).$$

Our goal is to construct a surrogate Q_{DNN} for Q and then to compute the expectation $\mathbb{E}[Q(\boldsymbol{\theta})]$ by MC sampling.

Multi-fidelity models and accuracy constraint. Suppose that we have a second-order accurate (in both time and space) finite difference scheme as the deterministic solver to compute realizations of $Q_{LF}(\boldsymbol{\theta})$ and $Q_{HF}(\boldsymbol{\theta})$ using a uniform grid with grid lengths h_{LF} and h_{HF} , respectively. We use the time step, $\Delta t = h/2$, to ensure stability of the numerical scheme, where the grid length h is either h_{LF} or h_{HF} , depending on the level of fidelity. Given a 1% failure probability and a decreasing sequence of tolerances $\epsilon_{TOL} = 10^{-1}, 10^{-2}, 10^{-3}$, a simple error analysis, similar to the analysis in [23], and verified by numerical computations, gives the minimum number of realizations $N_{\boldsymbol{\theta}}$ and the maximum grid length h_{HF} for the high-fidelity model required to achieve $\text{Prob}(\epsilon_{abs} \leq \epsilon_{TOL}) = 0.99$. Here, ϵ_{abs} is the absolute error given in (21). Table 5 summarizes the numerical parameters $(N_{\boldsymbol{\theta}}, h_{HF}, h_{LF})$, and the CPU time of evaluating single realizations of Q_{LF} and Q_{HF} . We choose $h_{LF} = s h_{HF}$, with $s = 1.6, 4, 8$, for the three tolerance levels.

Table 5: Required number of realizations and grid lengths to achieve $\text{P}(\epsilon_{abs} \leq \epsilon_{TOL}) = 0.99$.

ϵ_{TOL}	$N_{\boldsymbol{\theta}}$	h_{HF}	W_{HF}	h_{LF}	W_{LF}
10^{-1}	1.5×10^2	1/32	0.29	1/20	0.075
10^{-2}	1.5×10^4	1/128	10.50	1/32	0.21
10^{-3}	1.5×10^6	1/320	199.41	1/40	0.38

Surrogate construction. Following the RMFNN algorithm in Section 3.2, we first generate a uniform grid of $N = N_I + N_{II}$ points $\boldsymbol{\theta}^{(i)} \in [10, 11] \times [4, 6]$, with $i = 1, \dots, N$, collected into two disjoint sets Θ_I and Θ_{II} . We select the two disjoint sets so that $N \approx 11 N_I$, meaning that we need to compute the quantity $Q(\boldsymbol{\theta})$ by the high-fidelity model with grid length h_{HF} at 9% of points, i.e. $r = N_I/N \approx 0.09$; compare this with $r = 0.25$ in [23]. The number N of points will be chosen based on the desired tolerance, slightly increasing as the tolerance decreases, i.e. $N \propto \varepsilon_{TOL}^{-p}$ where $p > 0$ is small. In particular, as we observe in Table 6 below, the value $p = 0.2$ is enough to meet our accuracy constraints.

The architecture of *ResNN* consists of 2 hidden layers, where each layer has 20 neurons. The architecture of *DNN* consists of 4 hidden layers, where each layer has 30 neurons. The architecture of both networks will be kept fixed at all tolerance levels. For the training process, we split the available data points into a training set (95% of data) and a validation set (5% of data). We apply pre-processing transformations to the input data points before they are presented to the two networks. Precisely, we transform the points from $[10, 11] \times [4, 6]$ into the unit square $[0, 1]^2$. We employ the quadratic cost function and use the Adam optimization technique with an initial learning rate, $\eta = 0.005$. This learning rate is adapted during training by monitoring the MSE on the validation set. We do not use any regularization technique. Moreover, in order to take into account the uncertainty inherent in neural network training, each neural network is trained five separate times on five different random seeds. Table 6 summarizes the number of training-validation data N_I (for *ResNN*) and N (for *DNN*), the number of epochs N_{epoch} , batch size N_{batch} , and the average CPU time of training and evaluating the two networks for different tolerances over the five independent training trials. We remark that the variance in training and evaluation time is negligible across the different trials. With these parameters we construct three surrogates for Q_{DNN} , one at each tolerance level.

Table 6: The number of training data and training and evaluation time of the two networks

ε_{TOL}	N_I	N	<i>ResNN</i> : 2×20 neurons				<i>DNN</i> : 4×30 neurons			
			N_{epoch}	N_{batch}	W_{T_1}	W_{P_1}	N_{epoch}	N_{batch}	W_{T_2}	W_{P_1}
10^{-1}	324	3498	100	50	6.79	2.08×10^{-5}	500	50	62.84	5.80×10^{-5}
10^{-2}	451	4961	200	50	11.50	2.08×10^{-5}	1000	100	105.04	5.80×10^{-5}
10^{-3}	714	8003	1000	50	58.00	2.08×10^{-5}	5000	200	483.46	5.80×10^{-5}

Table 7 reports the MSE (18) in the constructed surrogates Q_{DNN} , using a uniform grid of $N_\varepsilon = 10^6$ points $\boldsymbol{\theta}$ in Θ , confirming that the (deterministic) MSE in the network approximation is comparable to the (statistical) absolute error ε_{abs} over all five training runs.

Table 7: MSE in the approximation $Q_{DNN}(\boldsymbol{\theta}) \approx Q(\boldsymbol{\theta})$.

ε_{TOL}	10^{-1}	10^{-2}	10^{-3}
ε_{MSE} (Trial 1)	2.05×10^{-3}	8.47×10^{-4}	4.20×10^{-4}
ε_{MSE} (Trial 2)	1.38×10^{-3}	2.04×10^{-3}	1.22×10^{-4}
ε_{MSE} (Trial 3)	4.64×10^{-3}	2.84×10^{-3}	4.34×10^{-4}
ε_{MSE} (Trial 4)	2.56×10^{-3}	3.21×10^{-3}	5.45×10^{-4}
ε_{MSE} (Trial 5)	2.19×10^{-3}	1.08×10^{-3}	1.03×10^{-3}

MC sampling. We now compute $\mathbb{E}[Q]$ by (19) and (20) and compare their complexities. Figure 11 (left) shows the CPU time as a function of tolerance. The computational cost of a direct high-fidelity MC sampling is proportional to $\varepsilon_{TOL}^{-3.5}$, following (15) and noting that the order of accuracy of the finite difference scheme is $q = 2$, and that the time-space dimension of the problem is $\gamma = 3$. On the other hand, if we only consider the evaluation cost of the RMFNN algorithm constructed surrogate, excluding the training costs, the cost of the proposed RMFNN method is proportional to ε_{TOL}^{-2} which is much less than the cost of high-fidelity MC sampling. When adding the training costs, we observe that although for large tolerances the training cost is large, as the tolerance decreases the training costs become negligible compared to the total CPU time. Overall, the cost of the proposed method approaches $\mathcal{O}(\varepsilon_{TOL}^{-2})$ as tolerance decreases, indicating orders of magnitude acceleration in computing the expectation compared to high-fidelity MC sampling. This convergence rate can also be seen by (17), noting that $\max(p + \gamma/q, 2 + \hat{p}) = \max(0.2 + 1.5, 2 + \hat{p}) = 2 + \hat{p}$, where $\hat{p} > 0$ is very small. We note that while we observe significant cost reductions at the tested tolerances, training neural networks to achieve very small tolerances can be challenging, and what is required to do this in practice, be it additional training data or optimization time is not rigorously understood [19]. Therefore, we do not assert that the demonstrated scaling will necessarily apply in these extremely small tolerance scenarios. Finally, Figure 11 (right) shows 20 instances of the relative error as a function of tolerance computed as 4 Monte Carlo simulations from each of the 5 independent network training runs. We see considerable variance in the network performance across different training runs, but even taking this variance into account, we meet the desired tolerance across all simulations.

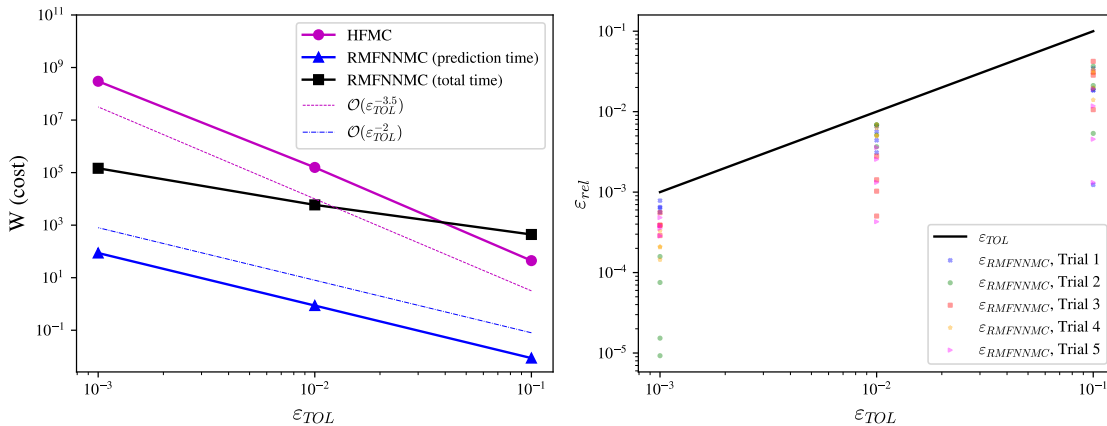


Figure 11: CPU time and error versus tolerance. Left: for large tolerances the training cost is dominant, making the cost of RMFNNMC more than the cost of HFMC. However, as tolerance decreases, the cost of RMFNNMC approaches $\mathcal{O}(\varepsilon_{TOL}^{-2})$; Right: relative error over different training trials as a function of tolerance verifies that the tolerance is met with 1% failure probability; different markers indicate 4 Monte Carlo simulations from each training trial

6 Conclusion

In this work, we presented a residual multi-fidelity computational framework that leverages a pair of neural networks to efficiently construct surrogates for high-fidelity QoIs described by systems of ODEs/PDEs. Given a low-fidelity and a high-fidelity computational model, we first formulate the

relation between the two models in terms of a possibly non-linear residual function that measures the discrepancy between the two model outputs. This modeling choice was motivated by a recently proved theoretical result [13], which guarantees the existence of ReLU networks approximating a large class of bounded target functions with minimal regularity assumptions to arbitrary tolerance with network complexity proportional to the uniform norm of the target function. This estimate provides general guidelines concerning when the developed modeling framework will be performative. When the residual function is small in uniform norm relative to the high-fidelity quantity, an approximating neural network *ResNN* can be constructed with lower relative network complexity. We hypothesize that this network can be effectively trained using a sparse set of high- and low-fidelity data, aligning with the typical conditions of most multi-fidelity modeling problems. The trained network *ResNN* is then used to efficiently generate additional high-fidelity data. Finally, the entire set of available and newly generated high-fidelity data is used to train a deep network, *DNN*, which acts as a cost-efficient surrogate for the high-fidelity QoI.

We presented four numerical examples to demonstrate the power of the proposed framework. In Example 5.1, we provided numerical justification for the inclusion of the low-fidelity model output in the input space of the residual function. We showed that this inclusion can yield a target function that is higher-dimensional, but with a simpler profile that can be learned by a network of lower complexity. In Example 5.2, we conducted a bi-fidelity surrogate construction task using three approaches: 1) the RMFNN algorithm, 2) the MFNN method from [23], and 3) a pure high-fidelity neural network without leveraging lower-fidelity information. Our results demonstrated orders-of-magnitude reduction in generalization error for the RMFNN surrogate compared to the other two methods. This performance advantage was most pronounced with sparse high-fidelity data, supporting our hypothesis linking reduced network complexity to improved training on sparse data. Moreover, in a multi-fidelity context, the RMFNN framework makes a meaningful improvement over the residual learning framework as formulated in ResNet [32]. Continuing, in examples 5.3 and 5.4 we used the RMFNN-constructed surrogate to approximate the expectation of our QoI via MC sampling. We demonstrated significant computational savings that increased as the desired error tolerance decreased, highlighting the efficiency of the RMFNN framework in reducing computational cost while maintaining accuracy.

One important future research direction concerns the extension of the RMFNN algorithm from bi-fidelity modeling to multi-fidelity modeling. The algorithm extends naturally in the case of an ensemble of lower-fidelity models that are strictly hierarchical in terms of their predictive accuracy for a given cost. In this case, we leverage a sequence of networks to learn a sequence of residual functions that efficiently generate additional high-fidelity data. The extension of the algorithm to more complex multilevel hierarchies of lower-fidelity models is an important open problem.

Declarations

- Data availability: Data sets generated during the current study are available at https://github.com/ondavis1997/residual_multifidelity
- Author contribution: All authors contributed meaningfully to the present work.

References

- [1] J. Schmidhuber. Deep learning in neural networks: An overview. *Neural netw.*, 61:85–117, 2015.

- [2] J. Sirignano and K. Spiliopoulos. DGM: A deep learning algorithm for solving partial differential equations. *Journal of Computational Physics*, 375:1339–1364, 2018.
- [3] E. Weinan and B. Yu. The deep Ritz method: A deep learning-based numerical algorithm for solving variational problems. *Commun. Math. Stat.*, 6:1–12, 2018.
- [4] E. Weinan, J. Han, and A. Jentzen. Algorithms for solving high dimensional PDEs: from nonlinear Monte Carlo to machine learning. *Nonlinearity*, 35(1):278, 2021.
- [5] J. Willard, X. Jia, S. Xu, M. Steinbach, and V. Kumar. Integrating physics-based modeling with machine learning: A survey. *arXiv:2003.04919*, 2020.
- [6] A. R. Barron. Universal approximation bounds for superpositions of a sigmoidal function. *IEEE Transactions on Information theory*, 39:930–945, 1993.
- [7] K. Hornik, M. Stinchcombe, and H. White. Multilayer feedforward networks are universal approximators. *Journal Neural Networks*, 2:359–366, 1989.
- [8] A. Pinkus. Approximation theory of the MLP model in neural networks. *Acta Numer.*, 8:143–195, 1999.
- [9] D. Yarotsky. Error bounds for approximations with deep ReLU networks. *Neural Networks*, 94:103–114, 2017.
- [10] D. Elbrächter, D. Perekrestenko, P. Grohs, and H. Bölcskei. Deep neural network approximation theory. *IEEE Transactions on Information Theory*, 67(5):2581–2623, 2021.
- [11] I. Daubechies, R. DeVore, S. Foucart, B. Hanin, and G. Petrova. Nonlinear approximation and (deep) relu networks. *Constructive Approximation*, 55(1):127–172, 2022.
- [12] I. Gühring, G. Kutyniok, and P. Petersen. Error bounds for approximations with deep ReLU neural networks in $W^{s,p}$ norms. *Analysis and Applications*, 18:803–859, 2020.
- [13] Owen Davis and Mohammad Motamed. Approximation power of deep neural networks: An explanatory mathematical survey. *Preprint, arXiv:2207.09511 v2*, 2024.
- [14] A. Jentzen, D. Salimova, and T. Welti. A proof that deep artificial neural networks overcome the curse of dimensionality in the numerical approximation of Kolmogorov partial differential equations with constant diffusion and nonlinear drift coefficients. *arxiv.org/abs/1809.07321*, 2018.
- [15] P. Grohs, F. Hornung, A. Jentzen, and P. Von Wurstemberger. A proof that artificial neural networks overcome the curse of dimensionality in the numerical approximation of black-scholes partial differential equations. *arXiv preprint arXiv:1809.02362*, 2018.
- [16] G. Kutyniok, P. Petersen, M. Raslan, and R. Schneider. A theoretical analysis of deep neural networks and parametric pdes. *Constructive Approximation*, 55(1):73–125, 2022.
- [17] P. Grohs and L. Herrmann. Deep neural network approximation for high-dimensional elliptic pdes with boundary conditions. *IMA Journal of Numerical Analysis*, 42(3):2055–2082, 2022.

- [18] M. Hutzenthaler, A. Jentzen, T. Kruse, and T.A. Nguyen. A proof that rectified deep neural networks overcome the curse of dimensionality in the numerical approximation of semilinear heat equations. *SN Partial Differential Equations and Applications volume*, 1, 2020.
- [19] Ben Adcock and Nick Dexter. The gap between theory and practice in function approximation with deep neural networks. *SIAM Journal on Mathematics of Data Science*, 3(2):624–655, 2021.
- [20] R.C. Aydin, F.A. Braeu, and C.J. Cyron. General multi-fidelity framework for training artificial neural networks with computational models. *Frontiers in Materials*, 6:1–14, 2019.
- [21] D. Liu and Y. Wang. Multi-fidelity physics-constrained neural network and its application in materials modeling. *Journal of Mechanical Design*, 141:121403, 2019.
- [22] X. Meng and G.E. Karniadakis. A composite neural network that learns from multi-fidelity data: Application to function approximation and inverse PDE problems. *Journal of Computational Physics*, 401: 20160751, 2020.
- [23] M. Motamed. A multi-fidelity neural network surrogate sampling method for uncertainty quantification. *International Journal for Uncertainty Quantification*, 10:315–332, 2020.
- [24] X. Meng, H. Babae, and G.E. Karniadakis. Multi-fidelity bayesian neural networks: Algorithms and applications. *Journal of Computational Physics*, 438:110361, 2021.
- [25] M. Guo, A. Manzoni, M. Amendt, P. Conti, and J.S. Hesthaven. Multi-fidelity regression using artificial neural networks: Efficient approximation of parameter-dependent output quantities. *Computer methods in applied mechanics and engineering*, 389:114378, 2022.
- [26] D.H. Song and D.M. Tartakovsky. Transfer learning on multifidelity data. *Journal of Machine Learning for Modeling and Computing*, 3(1), 2022.
- [27] A.A. Howard, M. Perego, G.E. Karniadakis, and P. Stinis. Multifidelity deep operator networks for data-driven and physics-informed problems. *Journal of Computational Physics*, 493:112462, 2023.
- [28] P. Conti, M. Guo, A. Manzoni, and J.S. Hesthaven. Multi-fidelity surrogate modeling using long short-term memory networks. *Computer methods in applied mechanics and engineering*, 404:115811, 2023.
- [29] L. Partin, G. Geraci, A.A. Rushdi, M.S. Eldred, and D.E. Schiavazzi. Multifidelity data fusion in convolutional encoder/decoder networks. *Journal of Computational Physics*, 472:111666, 2023.
- [30] F.J. Anscombe and J.W. Tukey. The examination and analysis of residuals. *Technometrics*, 5:141–160, 1963.
- [31] O. San and R. Maulik. Neural network closures for nonlinear model order reduction. *Advances in Computational Mathematics*, 44:1717–1750, 2018.
- [32] K. He, X. Zhang, S. Ren, and J. Sun. Deep residual learning for image recognition. In *IEEE Conference on Computer Vision and Pattern Recognition*, pages 770–778, 2016.

- [33] K. A. Cliffe, M. B. Giles, R. Scheichl, and A. L. Teckentrup. Multilevel Monte Carlo methods and applications to elliptic PDEs with random coefficients. *Comput. Visual Sci.*, 14:3–15, 2011.
- [34] F. Nobile and F. Tesei. A multi level Monte Carlo method with control variate for elliptic PDEs with log-normal coefficients. *Stoch PDE: Anal Comp*, 3:398–444, 2015.
- [35] M. Motamed and D. Appelö. A multi-order discontinuous Galerkin Monte Carlo method for hyperbolic problems with stochastic parameters. *SIAM J. Numer. Anal.*, 56:448–468, 2018.
- [36] A.-L. Haji-Ali, F. Nobile, and R. Tempone. Multi-index Monte Carlo: when sparsity meets sampling. *Numerische Mathematik*, 132:767–806, 2016.
- [37] M. C. Kennedy and A. O’Hagan. Predicting the output from a complex computer code when fast approximations are available. *Biometrika*, 87:1–13, 2000.
- [38] A. Forrester, A. Söbester, and A.J. Keane. Multi-fidelity optimization via surrogate modelling. *Proceedings of the royal society a: mathematical, physical and engineering sciences*, 463(2088):3251–3269, 2007.
- [39] M. G. Fernandez-Godino, C. Park, N. H. Kim, and R. T. Haftka. Review of multi-fidelity models. *arXiv:1609.07196*, 2016.
- [40] P. Perdikaris, M. Raissi, A. Damianou, N. Lawrence, and G. E. Karniadakis. Nonlinear information fusion algorithms for data-efficient multi-fidelity modelling. *Proc. R. Soc. A*, 473: 20160751, 2017.
- [41] P. Petersen and F. Voigtländer. Optimal approximation of piecewise smooth functions using deep ReLU neural networks. *Neural Networks*, 108:296–330, 2018.
- [42] Randall J LeVeque. *Finite difference methods for ordinary and partial differential equations: steady-state and time-dependent problems*. SIAM, Philadelphia, 2007.
- [43] M. Condon, A. Deaño, and A. Iserles. On systems of differential equations with extrinsic oscillation. *Discrete & Continuous Dynamical Systems - A*, 28:1345–1367, 2010.
- [44] Loukas Grafakos et al. *Classical Fourier analysis*, volume 2. Springer, New York, 2008.
- [45] G. S. Fishman. *Monte Carlo: Concepts, Algorithms, and Applications*. Springer-Verlag, New York, 1996.
- [46] A. Paszke et al. Pytorch: An imperative style, high-performance deep learning library, 2019.
- [47] F. Chollet et al. Keras. <https://keras.io>, 2015.
- [48] Y. Bengio. Practical recommendations for gradient-based training of deep architectures. In Müller KR, Montavon G., Orr G.B., editor, *Neural Networks: Tricks of the Trades*, pages 437–478. Springer, Berlin, 2012.
- [49] I. J. Goodfellow, Y. Bengio, and A. Courville. *Deep Learning*. MIT Press, Cambridge, MA, USA, 2016.